The Extratropical 40-Day Oscillation in the UCLA General Circulation Model. Part II: Spatial Structure

by

S. L. Marcus [1], M. Ghil[2], and J. O. Dickey[1]

[1] Space Geodetic Science and Applications Group
Jet Propulsion Laboratory
California Institute of Technology
Pasadena, California 91109-8099

[2] Department of Atmospheric Sciences
and Institute of Geophysics and Planetary Physics,
University of California, Los Angeles

November 1994

Submitted to *J. Atmos. Sci.*

Abstract

We examine intraseasonal oscillations in a three-year, perpetual-January simulation using a version of the UCLA GCM which produces no self-sustained Madden-Julian oscillation in the tropics. A robust, 40-day oscillation is found to arise in the model's Northern Hemisphere (NH) extratropics. Part I of this study (Marcus et al. 1994) addressed the zonally-averaged component of the GCM oscillation, manifested in wind- and pressure-induced variations in atmospheric angular momentum (AAM). Here we focus on the spatial features of the oscillation as manifested in the variability of the 500 mb height field,

A standing, wavenumber-two pattern is found in the NH extratropics, which undergoes tilted-trough vacillation in conjunction with the model's AAM oscillation. High (low) values of AAM are associated with low (high) 500 mb heights over the northeast Pacific and Atlantic oceans; the two centers' of action slightly different frequencies give rise to a long-period modulation (of about 300 days) in the amplitude of the intraseasonal oscillation. Global correlations with the leading empirical orthogonal functions (EOFs) of the NH extratropical 500 mb height field show northeast-southwest teleconnection patterns extending into the tropics, similar to those found in many observational studies. The zonally-averaged latent heating in the tropics exhibits no intraseasonal periodicity, but a 39-day oscillation is found in cumulus precipitation over the Western Indian Ocean. The latter shows significant coherence with EOF 1 but is absent in three shorter no-mountain experiments, indicating that it may be remotely forced by the intraseasonal oscillation arising in the NH extratropics of the standard-topography model.

1. Introduction and motivation

Since their discovery by Madden and Julian (1971, 1972), conceptual models for intraseasonal (40-50 day) oscillations in the tropics have generally invoked latent heat release as a driving force (Madden and Julian 1994). Intraseasonal oscillations subsequently detected in the extratropics (e.g. Krishnamurti and Gadgil 1985) have been interpreted by some investigators as a response to tropical forcing in the same frequency band (e.g., Anderson and Rosen 1983; Magaña and Yanai 199 1), implying that they share the same energy source. Recently, however, considerable evidence for an independent source of intraseasonal variability in the extratropics has accumulated. Liebmann and Hartmann (1984), for example, showed that 5-10 day averaged fluctuations in the 500 mb height field during northern winter were characterized by a southwest-northeast tilt, associated in quasi-geostrophic theory with equatorward energy propagation, and that they tended to precede the development of tropical convective disturbances, rather than follow them. Murakami (1988) documented the occurrence of southwest-northeast teleconnection patterns (his "NA" and "NP" surges) which appeared to regulate intraseasonal convective disturbances in the equatorial Indian and west Pacific oceans during Northern Hemisphere (NH) winter. Hsu et al. (1990) showed that sub-tropical Rossby wave trains could initiate convective activity in the equatorial Indian ocean in a case study of intraseasonal oscillations during the winter of 1985/86.

These observational and modeling results suggest that the origin for observed intraseasonal variability need not lie in the tropics. In this regard, Simmons et al. (1983) have found linearly unstable modes with periods near 50 days in a barotropic model linearized about the NH winter circulation at 300 mb and suggested that intraseasonal variability in the NH extratropics derives its energy from barotropic instability of the January mean circulation; in their model, the topography only contributes to the zonal asymmetry of the basic state. Ghil and colleagues [Ghil 1987; Ghil and Childress 1987

(PP. 164-201); Jin and Ghil 1990], on the other hand, have shown that oscillations in this frequency range may arise from the unstable interaction of nonzonal flow with the underlying topography. The dominant period of this instability in a nonlinear, equivalent-barotropic model using idealized NH topography (Legras and Ghil 1985) is near 40 days; however, for realistic parameter values it is characterized by aperiodic, intermittent behavior which accounts for the broadband nature of the observed intraseasonal variability.

Intraseasonal oscillations in both the tropics and extratropics have a strong signature in the axial component of' atmospheric angular momentum (AAM), which forms thereby a useful scalar diagnostic for low-frequency variability in the Earth-atmosphere system (e.g. Hide and Dickey 1991). While the strongest intraseasonal AAM signal is found in the tropics at periods near 50 days (Benedict and Haney 1988; Lau et al. 1989; Gutzler and Madden 1993), a smaller but distinct oscillation in AAM originates in the NH extratropics at periods near 40 days (Dickey et al. 1991; Magaña 1993). Phase propagation of AAM disturbances is largely polewards at periods near 50 days (Anderson and Rosen 1983); episodic equatorward AAM propagation is found, however, in the NH extratropics at periods near 40 days (Dickey et al. 1991). The latter AAM results, along with the model studies mentioned in the previous paragraph, support the existence of an independent intraseasonal oscillator in the NH extratropics, which may be capable of influencing the tropical atmosphere, at least on an intermittent basis.

In order to investigate this hypothesis in greater detail, Marcus et al, (1994 — hereafter MGD) examined AAM fluctuations arising in a series of perpetual-January experiments, made with a version of the UCLA general circulation model (GCM) which does not produce a vigorous Madden-Julian (MJ) oscillation in the tropics. In a three-year (1120-day) experiment employing standard topography, a robust, 42-day AAM oscillation was found to arise in the NH extratropics, while the model tropics showed no AAM periodicity. The extratropical GCM oscillation is similar in period and amplitude to that found by Dickey et al, (1991). This indicates that the 40-day oscillation observed in the

NH extratropics probably has a dynamical origin independent of the MJ mechanism, as it does in the GCM experiment employing standard topography, and in simple barotropic (Legras and Ghil 1985; Strong et al. 1993) and two-layer baroclinic (Keppenne and Ghil 1994) models. Three shorter GCM experiments, using different boundary or radiative forcing (see Table 1 of MGD) but with flat topography failed to show evidence of intraseasonal oscillations, indicating that the oscillation in the standard model originates from the interaction of the large-scale flow field with topography, as hypothesized by Ghil and colleagues.

In addition to oscillations with periods near 40 days, the standard-topography run of the GCM showed higher-frequency oscillations with periods near 21 days, which appear to be related to a westward-traveling wave with about this frequency observed in NH data at 500 mb by Branstator (1987) and Kushnir (1987), and modeled successfully by Keppenne and Ghil (1994). Ghil&dhfo(1991 a,b) have also studied an oscillation in this frequency range using NH 700 mb data, tropical outgoing long-wave radiation (OLR) data and Southern Hemisphere (SH) 500 mb data. While the no-mountain runs analyzed by MGD failed to show enhanced variability at 20-25 days, spectra of NH extratropical AAM from all three of these experiments had significant peaks in the 13—16 day range. The possible relationship of these variations with large-scale waves of similar period observed by Madden (1979) and with biweekly oscillations obtained in a barotropic model by Strong et al. (1993) remains a subject for future investigation.

In this study we concentrate on the dynamics of the 40-day oscillation in the standard topography experiment, focussing in particular on the spatial variability of the 500 mb height field. The mean and variance of the height field at 500 mb, along with composite maps keyed to the model's AAM oscillation, are presented in section 2. The leading empirical orthogonal functions (EOFs) of the NH extratropical 500 mb height field are presented in section 3, and correlation maps with the corresponding PCs are used to examine NH teleconnections with the tropics. In section 4 the EOFs of the 36-60 day

filtered height field and their relationship to the dynamics of the AAM oscillation are discussed. Regional variations of cumulus precipitation in the equatorial Indian and Pacific oceans on this time scale are examined in section 5, and a summary and discussion of the results of the study are presented in section 6.

2. Composite Analysis of 500 mb Height Variations

a. Climatology of the perpetual-January experiment

The mean 500 mb height field generated by the 1120-day standard run (see MGD for further details regarding the UCLA GCM and the conditions of the experiment) is shown in Fig. 1a, Agreement with the observed climatology is generally good, with troughs off the east coasts of Asia and the Americas and ridges over the west coasts of North America and Europe corresponding to observed features. The Southern Hemisphere, with little significant topography south of 40°S, shows a nearly zonal summer pattern, in agreement with observations. Further discussion of the model's ability to simulate the observed climate is found in Mechoso et al. (1987).

[Fig. 1 near here, please]

The mean 500 mb height field from the last 360 days of the longest no-mountain experiment (see Table 1 of MGD) is shown in Fig. 1 b. While the removal of the surface topography has little effect on the summertime flow field in the SH extratropics, the difference in the perpetual-January flow field of the NH extratropics is striking. The stationary ridges associated with the Rockies and Himalayas are almost entirely absent, while the ridge located over the west coast of Europe is greatly reduced in amplitude. The absence of NH extratropical oscillations from this run is consistent with the work of Jin and Ghil (1990), who find that such oscillations arise from the weakly-nonlinear interaction of quasi-resonant flow fields with the underlying topography.

b. Variance of the 500 mb height field

The root-mean-square (rms) height departures for the standard run are shown for the NH in Fig. 2a; the variability of the SH 500 mb height field is comparatively small during perpetual summer, and is not shown. Centers of maximum 500 mb variability, located over the northern Pacific and Atlantic oceans, are found on the eastern sides of the troughs associated with the jet exits from Asia and North America. The rms departure of the 36--60 day filtered height field for the NH is shown in Fig. 2b; the band-passed variance is even more strongly concentrated over the northern oceans, and is shifted slightly eastwards with respect to the total variance, closer to the downstream ridges located over the west coasts of North America and Europe.

[Fig. 2 near here, please]

The rms change from one day to the next of the 500 mb height field was computed for each day of the run, averaged over the region 200 N-900N on a reduced, equal-area grid similar to that employed by Barnston and Livezey (1987). The power spectrum for the resulting 11 19-day history of the 500 mb "phase-space velocity" (Legras and Ghil 1985; Ghil and Childress 1987) in the model's NH extratropics is shown in Fig, 2c. A broad peak is found between 36 and 60 days, coincident with the band of enhanced spectral power found in time series of AAM and Earth rotation data by Dickey et al. (1991); these two periods are used to define the limits of the intraseasonal band considered in the present study, as they were by Dickey et al. Two sharp peaks are found at periods of 25 and 19 days as well, separated in frequency by about twice the bandwidth associated with the spectral estimates, and hence statistically distinct. Distinct NHextratropical oscillations with periods of 23 and 17 days were also found in 700 mb height data by Ghil and Mo (1991a), and in AAM data from individual latitude belts by Dickey et al. (1991; their Fig. 11).

The ratio of the 36-60 day rms height variation to the total rms variation at 500 mb is shown in Fig. 3. Enhanced regions of intraseasonal variability are found in the northeast Pacific (NEP) and northeast Atlantic (NEA), corresponding to the two pronounced maxima of 36-60 day variability seen in Fig. 2b. In addition, regions of higher intraseasonal variability are also found extending southwestwards from the North American and European continents, into the central Pacific and Atlantic oceans, respectively. Similar features have been observed in the ratios of intraseasonal to total variability in OLR and 250 mb streamfunction data by Weickmann et al. (1985; their Figs. 1d and 2d), and by Magaña and Yanai (1991) in the 30-60 day variance of the 200 mb zonal wind field (their Fig. 2b). These similarities show that the 500 mb height data are representative of the intraseasonal oscillation in the extratropics, and that these extratropical features are well simulated by the UCLA GCM, in spite of the absence of a robust tropical MJ oscillation in this version of the model.

[Fig. 3 near here, please]

c. Composite maps associated with the AAM oscillation

In order to identify the dynamical features associated with the oscillation, composite maps of the unfiltered 500 mb height field were constructed, based on the 36--60 day filtered time series of the model's NH extratropical AAM. Composite maps keyed to the global AAM (not shown) were found to be quite similar to the composites based on the NH extratropical AAM, illustrating the central role played by the dynamics of that region in the model's global oscillation.

Fig. 4a presents a composite pattern for the entire run, formed by adding (subtracting) 500 mb maps for days with negative (positive) AAM departures greater than 1.5 times the standard deviation of the filtered AAM series. The resulting pattern indicates that strongly-positive height anomalies in both the NEP and NEA regions are associated with the low phase of the model's intraseasonal AAM cycle:

low AAM corresponds to weak westerlies, low index and blocked flow, cf. Namias (1950; see also Ghil and Childress 1987, Sees. 4.6, 5.3, 6.4, and 6.7). A pronounced southwest-northeast (SW-NE) tilt of the height anomalies in the NH extratropics is evident; patterns in the tropics and SH extratropics are much less distinct, although some indication of a coherent northwest-southeast (NW-SE) tilt is evident in the southern extratropics of the Western Hemisphere.

[Fig, 4 near here, please]

Fig. 4b shows a composite constructed from maps taken 12 days earlier than those incorporated in Fig. 4a, As such, it represents a pattern in approximate quadrature with the previous composite, with respect to the 36-60 day AAM oscillation. The tilt of the anomaly pattern in the NH extratropics has reversed from SW-NE to SE-NW, with some indication of a corresponding reversal in the SH extratropics. The GCM oscillation, therefore, exhibits a tilted-trough vacillation similar to that observed in a rotating, differentially-heatedannulus or dishpan by R. Hide, D. Fultz and their respective collaborators (e.g., Fultz et al. 1959; Hide 1977; Lorenz 1967; Ghil and Childress 1987, Chapter 5).

As opposed to amplitude vacillation, which is largely due to baroclinic energy conversions, tilted-trough vacillation involves mostly barotropic energy conversions. The patterns in Figs. 4a,b are thus consistent with a barotropic origin for the midlatitude 36--60 day oscillation, as hypothesized by Ghil (1987, 1988). It should be noted, however, that rotating-annulus experiments with wavenumber-two bottom topography have not produced, so far, a vacillation of this barotropic nature (Bernadet et al. 1990, and references therein).

The longitudinal position of the height anomalies in Figs. 4a and 4b is roughly constant, indicating that the model's intraseasonal AAM oscillation arises from a standing wavenumber-two pattern in the NH extratropics. In Fig. 4a, the SW-NE tilting pattern over the Atlantic is slightly stronger than over the Pacific. But

the reverse tilt (Fig. 4b) is much weaker in the Atlantic-European sector, and the positive-anomaly feature is displaced northeastward, from being centered over the British Isles to a center over Scandinavia. Since the NH topographic and thermal surface features are far from two-periodic, this is not too surprising, and must be related, at least in part, to the well-known differences between Pacific and Atlantic blocking.

The SW-NE tilting phase of the NH 30-60 day oscillation illustrated in Fig. 4a is also reminiscent of the extended-jet phase of the 250 mb streamfunction anomalies analyzed by Weickmann et al. (1985). Likewise, the NW-SE tilting phase of Fig. 4b appears to be related to the contracted-jet phase of Weickmann. In the model results shown here, however, the East Asian and North American jets are extended during roughly the same phase of the 30-60 day oscillation, while in the work of Weickmann and colleagues (their schematic Fig. 7) the former is most extended about one-quarter period ahead of the latter. The slight discrepancy in phasing is due apparently to Weickmann et al. (1985) keying their 250 mb anomalies to tropical OLR anomalies, which have a dominant wavenumber-one structure. These phase relationships are further discussed from the standpoint of the leading EOFS of the 500 mb height field in section 3.

Composite maps were also constructed for days 94-225 of the run, when the AAM oscillation in the NH extratropics was especially robust (cf. Fig. 7a of MGD). Figs. 5a-d show the anomaly composites associated respectively with the maximum, decreasing, minimum, and increasing phases of the AAM oscillation in the NH extratropics during this time, while Figs. 6a--d show the corresponding full composites, The standing wavenumber-two nature of the oscillation is generally well-maintained in the anomaly composites. In Fig. 5b, however, the positive anomaly in the NEA sector is shifted northward, leaving an elongated negative anomaly extending from North America across the Atlantic into northern Eurasia.

This pattern is similar to EOF 4 of NH winter 700 mb height data analyzed by Ghil and Mo (1991a — their Fig. 1 d), who found it to be associated with the 40-50 day oscillation in that region.

[Figs, 5 and 6 near here, please]

The meridional orientation of the height anomalies reverses during each quarter-cycle of the oscillation, with the anomalies over North America, in particular, aligned roughly perpendicular to the Rockies during AAM extrema, and parallel to the Rockies during phases of rapid AAM change. The sign of the anomalies reverses at each half-cycle, with high (low) heights located to the east of the Rockies and Himalayan Plateau during the increasing (decreasing) phase of the AAM oscillation. While the net torque on the atmosphere is small during the phases of AAM extrema, the surface pressure gradient across the Rockies and Himalayan Plateau exerts a net eastward (westward) torque on the atmosphere during the phases of increasing (decreasing) AAM (Marcus 1990). Recent studies using both observations (Weickmann et al. 1992) and GCM results (Boer 1990) have demonstrated a significant role for pressure torques in generating AAM fluctuations on intraseasonal time scales. The relationship between the tilted-trough vacillation cycle, surface pressure torques, and the dynamics of the NH extratropical oscillation in the UCLA GCM will be examined in greater detail in Part III of this study.

Similar oscillations have been found in numerical experiments performed by Legras and Ghil (1985), using a barotropic model with idealized NH topography. For a limited range of the constant thermal-wind forcing, regular oscillations with a period of 37 model days were obtained, The barotropic model oscillation is also characterized by a standing wavenumber-two pattern, and undergoes a similar form of tilted-trough vacillation (M. Kimoto. pers. comrnun., 1986). These results are confirmed by Tribbia and Ghil (1990), who used a more highly resolved equivalent-barotropic model than Legras and Ghil (1985) or Kimoto, with realistic global

topography. While the spatial details differ from those given by the GCM, the overall similarity of these results to the composites presented in Figs. 4-6 suggests that the GCM oscillation arises from the nonlinear interaction of the barotropic component of the flow field with topography (see also Jin and Ghil 1990).

3. Principal component analysis of the unfiltered height field

a. Leading EOFS of the 500 mb height field

The spatial characteristics of the model's intraseasonal oscillation were further investigated by an EOF analysis of the NH extratropical 500 mb height field. The leading EOFS are similar to the composites discussed above, and afford considerable insight into the dynamics of the oscillation. Examination of the corresponding principal component (PC) time series, in particular, provides an understanding of the ultra-low frequency behavior of the NH extratropical oscillation, and serves to highlight its interaction with variations in other regions of the global atmosphere.

Covariances for the 500 mb height field in the region 20°N--90°N were calculated on a reduced, approximately equal-area grid of 445 points, similar to that used by Barnston and Livezey (1987) for the Northern Hemisphere alone. The fractional variances associated with the first 20 EOFs are shown for the unfiltered and 36--60 day filtered heights by the solid and dashed lines, respectively, in Fig. 7. The efficiency of the description is considerably greater in the filtered case, with the first two EOFS containing *over* 50% of the variance. Shorter spatial scales are largely eliminated by the removal of the high-frequency portion of the fields; hence the larger spatial scales associated with the low-order EOFS account for a greater fraction of the variance for the time-filtered heights.

[Fig. 7 near here, please]

The first three EOFs for the unfiltered 500 mb heights are shown in Figs. 8a--c. Since the covariance rather than the correlation matrix was used, the leading EOFS have their maximum amplitudes near the centers of variability identified in Fig. 2a, EOFS 1 and 3, in particular, have their centers of activity located in the NEP and NEA regions, respectively, while EOF 2 shows evidence of a North-South seesaw and a wavenumber-three pattern in the zonal direction.

[Fig. 8 near here, please]

Both EOFS 1 and 3 show a distinct SW-NE tilt, similar to that seen in the composite depicting the 500 mb height difference between the extremes of the AAM cycle in the NH extratropics for the full run (Fig. 4a). EOF 1, in particular, resembles the composite patterns over the Pacific and North America, while EOF 3 resembles the composite patterns over the Atlantic and Eurasia. While these two EOFS represent, therefore, variability associated with the model's 36----60 day AAM oscillation, EOF2 shows no distinct meridional tilt, and little resemblance to the 36-60 day AAM composites.

Power spectra for PCS 1 and 3 are shown in Fig. 9a by solid and dashed lines, respectively, while the power spectrum for PC 2 is shown in Fig, 9b (note difference in vertical scales). Both PCs 1 and 3 show spectral peaks in the 36-60 day range. The peak for PC 1, associated with variability centered upstream from the Rockies (cf. Fig, 8a), lies within a bandwidth of the 42-day peak obtained for the NH extratropical AAM series by MGD (their Fig. 5). The peak for PC 3 has slightly less power than the PC 1 peak, although its level of statistical significance is higher (95% vs 90% for the PC 1 peak). It is separated by about a bandwidth from the PC 1 peak and may represent a distinct oscillation, as suggested by the AAM analysis of Penland et al. (1991) that showed two distinct peaks in an analysis of 810 pentads (4050 days) of global AAM, at 48.5 and 51.0 days.

[Fig. 9 near here, please]

PCs 1 and 2 also show enhanced variability at higher frequencies. The 21.5-day and 15-day peaks for PC 1 are significant at the 95% level, while PC2 shows its most significant departure from a red-noise process (80910) at a period of 25 days. Composite 500 mb maps keyed to the 16-24 day global filtered AAM (not shown) exhibit a clear wavenumber-three pattern in the NH mid-latitudes, similar to that shown by EOF 2. Branstator (1987) identified a 23-day oscillation in 500 mb height data which had maximum amplitude over Canada. These higher-frequency oscillations, therefore, may arise from the interaction of relatively shorter atmospheric waves with topography, and necessitate the analysis of multi-level fields (cf. Keppenne and Ghil 1994; Strong 1994).

The coherence estimate for PCs 1 and 3, shown in Fig. lOa, exhibits a maximum centered at 39 days, significant at the 99% level; another, sharper peak is found near 15 days. The corresponding phase difference (Fig. 10b) shows that, over the intraseasonal (36—60 day) band, variations in PC 1 tend to lead those in PC 3 by about six days. This is consistent with the composite life cycle of Weickmann et al. (1985), as discussed in section 2c, and suggests that intraseasonal variations in the NEA region may partially reflect the upstream influence of topographically-generated disturbances in the NEP region.

[Fig. 10 near here, please]

The coherence between PCs 1—3 and the time series of AAM from the model's NH extratropics is shown in Figs. 11a-c, respectively. PCs 1 and 3 both show peaks significant at the 99% level near periods of 40 days, indicating that EOFS 1 and 3 of the 500 mb height field in the NH extratropics, along with the AAM for that region, all participate in the model's 40-day oscillation, In addition, PC 3 shows highly significant coherence with the AAMataperiodof51 days; this peak is well separated from the 40-day coherence peak, but is statistically indistinguishable in frequency from the 52.5-day spectral peak shown by PC 3 (Fig.

9a), from the 5 1.O-day peak of global AAM in Penland et al. (1991), and from the 50-day spectral peak found for tropical AAM by Dickey et al. (1991). This evidence supports the existence of a separate oscillation with a period near 50 days in the NEA region (cf. Fig. SC), which may also be involved in tropical-extratropical interaction on this time scale.

[Fig, 11 near here, please]

b. Correlation of PCs with the global 500 mb height field

The EOFS above were defined for 500 mb heights in the NH extratropics (200 N—90°N). Correlations of the global 500 mb height field with the corresponding PCs can serve, therefore, to highlight relationships between the NH midlatitudes and other areas of the globe. Figs, 12, 13, and 14 present correlation coefficients between 500 mb heights and PCs 1, 2, and 3 respectively, at different lags. An arbitrary sign reversal was applied to the EOFs shown in Fig. 9 before computing the correlations; this emphasizes, as we shall see, teleconnections with the tropics.

[Fig. 12 near here, please]

The first three PCs were found to have decorrelation times of 4.3, 3.9, and 7.2 days, respectively. Decorrelation times for the 500 mb height anomalies vary from point to point over a similar range. If both data types are conservatively assigned a decorrelation time of 7.2 days, the standard deviation of the estimated correlation coefficient between the two data types under a null hypothesis of zero true correlation is about 0.08 (see MGD, section 3b, for details of the statistical assumptions made here). The subsequent correlation maps, therefore, use a contour interval of 0.08, with contours starting at (plus or minus) 0.16. The contoured areas therewith roughly indicate correlations significant at the 95% level.

For the height field leading PC 1 by six days (Fig, 12a) a significant area of positive correlation occurs over Siberia, showing a distinct SW-NE tilt. A weak

North-South correlation dipole is also found in the central North Pacific. At this lag, however, significant correlations are generally restricted to the NH extratropics. For the height field leading PC 1 by three days, the North-South dipole has strengthened (Fig. 12b), and significant correlations now occur in the tropical mid-Pacific. The SW-NE axis of high correlation over Siberia has also strengthened and has extended southwestwards over the Arabian peninsula, with significant correlations now covering the western half of the Indian Ocean down to a latitude of 100S. A similar pattern has been derived by Murakami (1988) from composite 30—60 day variations in the 850 mb streamfunction, keyed to eastward-propagating convective anomalies in the tropical Indian and west Pacific oceans during NH winter (his "NA" burst). The occurrence of this feature in the perpetual-January run increases our confidence in the realism of the intraseasonal variability simulated by the GCM, and underscores the extratropical origin of the teleconnection pattern described by Murakami (1988).

The simultaneous correlation of the 500 mb height field with PC 1 (Fig. 12c) resembles, of course, the corresponding EOF in the NH region (Fig. 8a — note sign reversal). The area of positive correlation located over the northeast Asian coastline bears a strong similarity to 850 mb correlation patterns associated with outbreaks of polar air into the East China Sea obtained by Sumathipala and Murakami (1988). These outbreaks may also be associated with intensified convection in the far western tropical Pacific (Chang and Lau 1982; Hsu et al. 1990), providing a potential link between NH extratropical dynamics and the development of intraseasonal tropical convective disturbances,

The largest correlation values at zero lag (Fig. 12c) are found in the North-South dipole occupying the mid-Pacific. The correlation maximum centered at 200N, 170°W is coincident with the isolated maximum of 36-60 day fractional variance at 500 mb obtained in Fig, 3 here and with maxima in fractional 28-72 day

variance in OLR and 250 mb streamfunction fields found in multi-year data sets by Weickmann et al. (1985). This area also coincides with the preferred location of the mid-Pacific trough, which serves as a conduit for tropical-extratropical interactions on the 30-60 day time scale (Magaña and Yanai 1991), The presence of this activity center in a GCM simulation with no sustained MJ oscillation, therefore, as well as its high correlation with PC 1 of the NH extratopical 500 mb height field, indicates that a substantial part of this interaction may originate in the extratropics.

When the 500 mb height field lags PC 1 by three days (Fig. 12d), the correlation maxima found at lag zero over North America and the mid-Pacific (cf. Fig. 12c) join into a single coherent pattern, extending southwestwards from Hudson Bay to New Guinea in the western equatorial Pacific. A similar pattern is documented by Murakami (1988) in 30–-60 day composites of the 200 mb streamfunction keyed to intraseasonal OLR disturbances during NH winter (his category-3), again indicating that the GCM captures a substantial part of the observed intraseasonal NH winter variability: even in the absence of the MJ oscillation.

The correlation with the 500 mb height field lagging PC 1 by six days (Fig. 12e) does not progress further eastward, but decays in place, i.e. large-scale correlations with PC 1 do not propagate beyond North America, Similarly, the area of high correlation located over Siberia leading PC 1 by six days (Fig. 12a) propagates only to the East Asian coastline before decaying. The major correlation center located over the NEP also moves only slightly eastwards before decaying. The oscillation associated with EOF 1, therefore, appears to be primarily standing, in agreement with the conclusions of sections 2b and c.

The correlation pattern obtained with the 500 mb height field leading PC 2 by six days (Fig. 13a) shows a North-South seesaw, with only a little of the wavenumber-three pattern characterizing EOF 2 (Fig. 8b) present, and a deep trough

over Central Asia. With the height field leading PC 2 by three days (Fig. 13b) the wavenumber-three pattern becomes evident, although the center over Japan is displaced westwards from the corresponding North Pacific maximum of the EOF pattern, while the Central Asian trough has moved perceptibly eastwards. The simultaneous correlation pattern (Fig. 13c) closely mimics EOF 2 (Fig. 8b — note sign reversal), although the North-South seesaw is stronger in the correlation map than in the EOF. Moreover, the features here are quite pronounced over Eurasia, while EOF 2, like the Branstator (1987) wave, is strongest over North America, and the evidence here points to eastward, rather than westward propagation. In contrast with the simultaneous pattern obtained for EOF 1 (Fig. 12c), correlations with the tropics are quite weak.

[Fig. 13 near here, please]

With the 500 mb height field lagging PC 2 by three days (Fig. 13d), a tongue of positive correlation extends southwestwards from North America into the Pacific, with a weaker amplitude but the same orientation as a similar belt seen in the correlations with PC 1 (e.g., Fig. 12d). At a lag of six days (Fig, 13e) the tropical correlations of 500 mb height with PC 2 become most evident, showing also a mid-Pacific dipole similar to that obtained with PC 1 (Fig. 12a).

With the 500 mb height field leading PC 3 by six days (Fig. 14a), a North-South dipole is visible in the eastern North Atlantic, similar to the correlations obtained above with PCs 1 and 2 in the Pacific. As the lead for the height field is reduced to three days (Fig. 14b) and to zero days (Fig. 14c), the dipole intensifies and becomes joined to an area of high correlation centered over the eastern Mediterranean, giving rise to an elongated feature extending southwestwards from central Asia into the subtropical Atlantic. These features are similar to the SW-NE trending correlations obtained with PC 1 from Siberia into the Indian Ocean (Fig. 12b) and from North America into the sub-tropical Pacific (Fig. 12d), implying that

similar dynamic interactions link the extratropics and tropics over the Atlantic, Indian, and Pacific oceans in the model.

[Fig. 14 near here, please]

Simultaneous correlations with PC 3 are also found extending southwestwards from North America into the West Pacific, resembling those obtained with PC 1 at a lag of six days. This is consistent with the six-day lag found in the coherence estimate for PCs 1 and 3 in the 36--60 day frequency range (Fig. 10b). EOFS 1 and 3 represent manifestly two different phases of the NH 36--60 day oscillation, about six days apart. Their not being one-quarter period out-of-phase, nor spatially in quadrature, indicates clearly the nonlinear character of the oscillation, in agreement with the theoretical work of Ghil (1987), Jin and Ghil (1990) and Tribbia and Ghil (1990).

The zero-lag correlation pattern with PC 3 (Fig. 14c) is particularly reminiscent of the 250 mb streamfunction-anomaly composite of Weickmann et al. (1985) for their positive Atlantic index phase (their Fig. 9d); very slight shifts in pattern are clearly due to the difference in height level, field variable and phase within the oscillation. In a comparison of tropical OLR variations with 500 mb data from the NH extratropics, Liebmann and Hartmann (1984) found that height anomalies with a SW-NE tilt were correlated with equatorward wave energy propagation and the subsequent enhancement of convective activity to the southeast. This is consistent with the findings of Weickman et al. (1985), who demonstrated that similar height anomalies (their Fig. 9d) tend to be followed by enhanced convection over equatorial Africa and the Western Indian Ocean, initiating another cycle of the MJ oscillation.

The correlation pattern with the 500 mb height field lagging PC 3 by three and six days (Figs. 14d,e) shows slight southeastward propagation towards the Indian ocean, consistent with the equivalent-barotropic Rossby wave originating in

the Atlantic documented by Hsu et al. (1990 -– their Fig. 6). They showed that the arrival of a region of ascent associated with this wave triggered large-scale cumulus heating in the western Indian ocean, giving rise to subsequent downstream convective anomalies associated with the development of the 1985/86 intraseasonal oscillation. The occurrence of a similar wave train in this version of the UCLA GCM with no MJ oscillation suggests that variability originating in the extratropics may play a key role in modulating the equatorward flux of wave energy, and lead to the initiation of nearly periodic flare-ups of convective activity in the tropics.

4. PC analysis of the filtered height field

a. Relationship of leading intraseasonal EOFS to MM variations

In order to focus on the dynamics of the model's AAM oscillation, the 500 mb height field at all grid points was filtered to retain variations in the 36-60 day band. The first three EOFs of the filtered height field in the NH extratropics (hereafter referred to as EOFFs) are shown in Figs. 15a-c. The NEP and NEA centers of action (Fig. 2b) are emphasized, as for the unfiltered EOFs (Figs, 8a-c). EOFFS 1 and 2 represent approximately in-phase and out-of-phase fluctuations of these two centers, respectively; together they account for more than 50% of the variance of the filtered heights in the NH extratropics (Fig, 7, dotted line).

[Fig. 15 near here, please]

EOFF 1, in particular, bears a strong resemblance to the composite pattern associated with the difference bewteen the low and high phases of the intraseasonal AAM cycle (Fig. 4a). Not surprisingly, therefore, the correlation between the comesponding PC (referred to as PCF 1) and the filtered NH extratropical AAM at small lags is strongly negative (see Fig. 16), reaching an amplitude of-0.82 with the PCF 1 leading by two days. The pattern for EOFF 1 resembles that for EOF 1 (of the unfiltered 500 mb heights) over the Pacific and North America, and that for

EOF 3 over the Atlantic and Eurasia. The amplitude of PCF 1, and hence of the AAM oscillation, is therefore largest when PCs 1 and 3 (of the unfiltered heights) oscillate approximately in phase. In this connection, it is worth noting that the beat frequency between the intraseasonal peaks for PCs 1 and 3 (Fig, 9a) is approximately 300 days, similar to the approximate periodicity for the envelope of the AAM oscillation (see Fig. 7 of MGD). It is likely, therefore, that the model's amplitude-modulation cycle originates from the slightly different intraseasonal frequencies associated with the NEP and NEA centers of variability (see also Penland et al. 1991).

[Fig. 16 near here, please]

The leading PCFS have, *a priori,* most of their variance in the 36—60 day band. Due to the orthogonality constraint, therefore, PCFS 1 and 2 oscillate in quadrature with each other. Because of the high correlation of PCF 1 with the filtered NH extratropical AAM, therefore, PCF 2 has only a small correlation at zero lag with this AAM series (Fig, 16), Hence, the out-of-phase fluctuations of the NEP and NEA centers characterizing EOF 2 (Fig. 15b) contribute little to the overall strength of the 36—60 day AAM oscillation.

EOFF 3 shows both a North-South seesaw and a wavenumber-three pattern in the zonal direction (Fig. 15c), and bears a marked similarity to EOF 2 for the unfiltered 500 mb heights (Fig. 8b). While the time variability for PCF 3 (not shown) is mostly confined –- due to the pre-filtering -— to the 36--60 day band, the power spectrum for PC 2 shows its greatest departure from red noise at a period of 25 days (Fig. 9b). The similarity between the spatial patterns of EOF 2 and EOFF 3 suggests, therefore, that this mode may be involved in the nonlinear interaction of the 36-60 day band with higher-frequency oscillations (cf. Jin and Ghil 1990; Tribbia and Ghil 1990).

b. Correlation of PCFs with the filtered 500 mb height field

Global correlations of the 36-60 day filtered 500 mb height field with the first three NH PCFS are presented in Figs. 17-19, The plotted contours begin at plus and minus 0.40, and an arbitrary sign reversal has been applied, in order to emphasize correlations with the tropics, as in Figs. 12—14. Formal significance levels are not presented, since the emerging patterns correspond to physical features corroborated by other results.

With the height field leading PCF 1 by six days (Fig. 17a), the wavenumber-two pattern characterizing the corresponding EOFF (Fig, 15a — note sign reversal) is apparent in the NH extratropics, and shows a pronounced NW-SE tilt. Correlations in the tropics are virtually absent, with the exception of a mid-Pacific dipole pattern similar to those found for the unfiltered EOFs. With the height field leading PCF 1 by three days (Fig. 17b) the wavenumber-two pattern in the NH extratropics intensifies, while the meridional tilt seen in Fig. 17a is less evident, Extensive areas of positive correlation are now found in the tropics, extending from equatorial Africa into the Indian and West Pacific oceans, and terminating in an intense correlation maximum found in the sub-tropical central Pacific. Note that this pattern resembles the correlation dipole found with PC 1 (Figs. 12b,c), consistent with the large 36—60 day variance fraction found in this region,

[Fig. 17 near here, please]

At zero lag the meridional tilt of the anomalies in the NH extratropics begins to reverse (Fig. 17c), while the positive correlations have completely covered the tropics. With the height field lagging PCF 1 by three days (Fig. 17d) the wavenumber-two pattern in the NH extratropics takes on a distinct SW-NE tilt, although the intensity of the pattern has weakened somewhat, The correlations in the tropical belt, on the other hand, have reached their maximum intensity, with the highest values for the globe now located in the tropical mid-Pacific. With the height

field lagging PCF 1 by six days (Fig. 17e) the correlations in the tropical belt remain strong, although the pattern in the NH extratropics, where the corresponding EOFF is defined, has almost disappeared,

The meridional tilt of the NH extratropical correlations with PCF 1 changes from SE-NW at a lead of six days (Fig. 17a) to SW-NE at a lag of three days (Fig. 17d), when the zonally symmetric, negative height departure in the tropics reaches its maximum amplitude, and the NH extratropical AAM is at its minimum (cf. Fig. 16a). Thus, the tilted-trough vacillation cycle in the NH extratropics appears to be associated with the zonally symmetric anomalies in the tropics discussed by MGD (their section 3g). Note that the longitude of the NH extratropical correlation centers remains fixed as their meridional tilt changes from SW-NE to SE-NW during the quarter-phase of the tilted-trough cycle shown here, in keeping with the standing nature of the oscillation.

With the filtered 500 mb height field leading PCF 2 by six days (Fig. 18a) the pattern characterizing EOFF 2 is already visible in the NH region (note sign reversal from Fig. 15b), although the North Pacific center is relatively weak and is shifted westwards from its main location. Correlations in the tropics are well-developed, and bear a strong resemblance to the negative of the tropical correlations obtained with EOFF 1 at a lag of six days (Fig. 17e). This is consistent with the 12-day lag existing between PCF 1 and the negative of PCF 2 (Fig. 16b); indeed, the smaller magnitude of the correlations obtained here indicates that the variations in EOFF 1 — with the Pacific and Atlantic anomalies in phase, rather than in EOFF 2, where they are out-of-phase -- are driving the zonally symmetric oscillation in the model tropics.

[Fig. 18 near here, please]

With the filtered 500 mb height field leading PCF 2 by three days (Fig. 18b), the tropical correlation pattern has weakened considerably. The intense dipole

visible in the Eastern Atlantic at a lead of 6 days (Fig. 18a) is still in evidence, however, and resembles strongly the correlation patterns obtained in that area with EOF 3 (Fig, 14c — note that EOF 3 has a positive center while EOFF 2 is negative in this area). The resemblance between the correlation patterns of PC 3 with the unfiltered heights and PCF 2 with the filtered heights is consistent with the strong intraseasonal variability shown by PC 3 (dashed line in Fig. 9a).

Correlations of the filtered 500 mb height field computed simultaneously with or three days after PCF 2 (Figs. 18c,d respectively) show decreasing areas of significance in the tropics. This confirms that the tropical correlation features arise indirectly, through the phase relationship between PCF 2 and PCF 1 shown in Fig. 16b. The correlation with the filtered 500 mb heights lagging six days behind PCF 2 (Fig. 18e) resembles that obtained with the heights leading PCF 1 by six days (Fig. 17a), consistent with the 12-day lag of PCF 1 behind the positive phase of PCF 2 (left half of Fig. 16b).

Since the variance carried by EOFF 3 is considerably less than that associated with the two leading EOFFs of the filtered 500 mb height fields (Fig. 7), the correlation levels of the global height field with PCF 3 (Figs. 19a-e) are generally less than those for the first two PCFs. While the simultaneous correlation pattern resembles EOFF 3 (Fig. 15c, with a change in sign), little significant correlation with other areas of the globe is found. The correlatons at lags or leads of three and six days resemble the simultaneous pattern, with the magnitude of the correlations decaying as the lag or lead increases.

[Fig, 19 near here, please]

While the largest correlations with the PCFS occur in the NH extratropics and the tropics, it is intriguing to note pronounced tongues of positive correlation with the height field lagging PCF 1 (Figs. 17c—e) and leading PCF 2 (Figs. 18a—c) in the SH mid-latitudes. These tongues have a general NW-SE orientation and a

wavenumber-three structure (compare Mo and Ghil 1987), occurring just west of Australia and of South America, and west of or over South Africa, In addition, one area of large positive correlation with the height field leading PCF3 is found in the SH mid-latitudes (Figs. 19a–-c), namely the Tasman Sea and New Zealand. This is an area of pronounced SH blocking (e.g., Trenberth and Mo 1985),

5. Interaction of cumulus heating with dynamical variability

The extensive spatial correlations obtained between the tropical 500 mb height field and PCF 1 (Figs, 17c—e) indicate that a zonally symmetric oscillation in the model tropics is associated with the standing wavenumber-two pattern represented by EOFF 1 in the NH extratropics. Fig. 20 shows the lag correlation between PCF 1 and the area-averaged 500 mb height anomaly for the tropics (200S—20°N), filtered in the 36—60 day band. The strong correlation (-0.86 with PCF 1 leading by three days — recall sign change in Fig. 17d) indicates that variations in the model are closely coupled to the dynamics of the NH extratropics on intraseasonal time scales. MGD showed that this relationship takes the form of a meridional exchange of mass between the tropics and NH extratropics, occurring in conjunction with the AAM oscillation in the latter region. MGD further demonstrated the lack of sustained intraseasonal variations in the tropics' zonally averaged latent heating; the model's tropical oscillation is thus driven dynamically, rather than thermodynamically.

[Fig. 20 near here, please]

A search was also made for intraseasonal variations in convective activity in the Indian and Western Pacific Oceans, where the OLR signature of the MJ oscillation is clearest. Figs. 21 a—f show spectra for cumulus precipitation from six regions measuring 24 degrees latitude by 25 degrees longitude, centered along the equator between longitudes 55°E and 60°W. The first of these regions, occupying

the Western Indian Ocean and coinciding approximately with the area of 500 mb heights found to be significantly correlated with PC 1 at a lead of three days (Fig. 12b), shows a distinct peak at a period of 39 days (Fig. 21a), significant at the 95% level with respect to an AR 1 process (see MGD for details of the statistical model), Since the spectral peak for PC 1 occurs at 45 days (Fig. 9a), the model oscillation coincides well in frequency with an observed enhancement of summer precipitation in southern India found by Hartmann and Michelsen (1989) at periods of 40—45 days.

[Fig. 21 near here, please]

The coherence between PC 1 and the cumulus precipitation in the western Indian Ocean (henceforth denoted as WIOCP) is plotted in Fig. 22. The largest peak for the frequency range shown is at 45 days, within a bandwidth of the NH AAM oscillation frequency (see Fig. 5 of MGD). The maximum coherence is significant at the 95% level, while the phase difference between PC 1 and WIOCP (not shown — see, however, Marcus 1990, Fig. 60) is not significantly different from zero. Comparison with Fig. 12b, therefore, indicates that cumulus convection in the western Indian ocean tends to be enhanced about three days after the passage through that region of a trough associated with EOF 1 of the NH extratropical 500 mb height field (recall the sign reversal applied to the correlations computed from the EOFs). Given the lack of a sustained MJ oscillation in the perpetual-January simulation, therefore, the most likely source of nearly periodic excitation for the model's convective activity in this region is the intraseasonal oscillation arising in the NH extratropics.

[Fig. 22 near here, please]

A comparison of WIOCP spectra from the three no-mountain experiments (see Table 1 of MGD) with similar spectra from the standard-topography experiment (see Fig. 23) confirms this hypothesis. None of the spectra from the no-mountain

runs show peaks within a bandwidth of the WIOCP oscillation in the standard-topography experiment, while spectra for three 315-day segments of the standard experiment, chosen to have approximately the same length as the average duration of the no-mountain runs, all, have WIOCP peaks within this range, While none of the peaks in Fig. 23 are statistically significant due to the shortness of the records considered (the first 40 days were dropped from each no-mountain run to eliminate transients), these results imply that the intraseasonal WIOCP peak in the full 1120-day standard experiment (which is significant at the 95% level) arises from the interaction of the extratropical flow field with topography, as does the 40-day AAM oscillation,

[Fig. 23 near here, please]

The spectra for cumulus precipitation in regions 2-6 from the standard-topography run (Figs. 2 lb-f) do not show any significant peaks in the 36-60 day band. Considerable activity is evident in the 16-24 day band, however, as was found for global AAM variations by MGD. In particular, significant peaks in cumulus precipitation are found at periods of 20 and 16.5 days over the Maritime Continent (Fig. 2 1c) and New Guinea (Fig. 2 Id) regions, respectively. These may be related to higher-frequency modes, at 20—25 and 1&17 days, found in tropical observations (e.g., Ghil and Mo 199 la; Hartmann et al. 1992). Cumulus parameterization schemes employed in GCMS, on the other hand, often produce vertical heating profiles with excessive equivalent depth, that lead to unrealistically high frequencies in the tropics (e.g., Hayashi and Sumi 1986; Lau and Lau 1986; Neelin et al. 1987; Pitcher and Geisler 1987), and a similar tendency exists in this version of the UCLA GCM (Tokioka et al. 1988), An improved cumulus scheme with convective downdraft pararneterization (Cheng and Arakawa 1991 1993), currently under development, is expected to produce a more realistic MJ simulation in the UCLA GCM; it should afford the opportunity to examine the interaction

between tropical and extratropical intraseasonal variability in a model in which the two variabilities are equally well represented.

6. Concluding remarks

a. Summary

We have studied the dynamics of intraseasonal oscillations in a version of the UCLA GCM which does not exhibit a sustained Madden-Julian (MJ) oscillation in the tropics. The zonally symmetric aspects of the oscillation, particularly as they pertain to atmospheric angular momentum (AAM) variations, were investigated in Part I of this study (Marcus et al. 1994, referred to as MGD throughout the main text here). They found a robust, 42-day oscillation in the NH extratropics during a three-year "perpetual-January" experiment, accompanied by a barotropic, zonally symmetric oscillation in the tropics. No periodicity was found in the zonally averaged tropical latent heating, however, confirming that the model oscillation is driven dynamically, rather than thermodynamically. Three shorter "no-mountain" experiments failed to produce intraseasonal oscillations, consistent with a topographic origin as hypothesized by Ghil and colleagues [Ghil 1987; Ghil and Childress 1987 (pp. 164-201); Jin and Ghil 1990].

In the present part II of the study we address the spatial aspects of the model's 40-day oscillation, focussing in particular on the NH extratropical 500 mb height field and its teleconnections with other areas of the globe. The mean 500 mb height field in the standard-topography experiment is characterized by ridges over the western coasts of North America and Europe and *over* the Tibetan plateau, in agreement with observations. These features are virtually absent in the no-mountain experiments, however, which are characterized by nearly zonal flow (see Fig. 1). The lack of intraseasonal oscillations in the no-mountain runs is consistent with the work of Jin and Ghil (1990), who found them to arise from the weakly-nonlinear interaction of quasi-resonant flow with the underlying topography.

Intraseasonal variations in the 500 mb height field are concentrated primarily over the northeastern Pacific (NEP) and Atlantic (NEA) oceans, respectively (see Fig. 2), A map of the ratio of intraseasonal to total variance in the model's 500 mb field (Fig. 3) shows considerable resemblance to patterns found by other investigators in OLR and 250 mb streamfunction data, indicating that the 500 mb field representative of the intraseasonal oscillation. The oscillation is characterized by a standing wavenumber-two pattern in the NH extratropics (Fig. 4), which undergoes tilted-trough vacillation in conjunction with the model's AAM cycle. The tilt changes from SW-NE, when the AAM is maximum or minimum, to SE-NW when it is decreasing or increasing; the largest height gradients are located over major topographic features (i.e., the Rockies and Tibetan plateau; see Fig. 5). A detailed analysis of the torques responsible for the AAM oscillation will be presented in Part 111 of this study.

The first and third EOFS of the unfiltered 500 mb height field in the extratropics are concentrated in the NEP and NEA regions, respectively (Fig. 8). Power spectra of the corresponding PCs both show peaks in the intrase asonal range, with EOF 3 having a slightly longer period (Fig. 9), and tending to lag behind EOF 1 by about six days (Fig. 10). The second EOF has a wavenumber-three pattern, with the spectrum of the corresponding PC showing its most significant departure from red noise at a period of 25 days; these higher-frequency oscillations may be related to the 23-day wave found by Branstator (1987) and Kushnir (1987), and to oscillations of similar period documented by Ghil and Mo (1991a).

The first EOF of the 36-60 day filtered height field (EOFF 1) represents in-phase variations between the NEP and NEA centers, while EOFF 2 is characterized by out-of-phase variations of the two (Fig, 15). The large (negative) correlation of PCF 1 and very small correlation of PCF 2 with the filtered AAM time series (Fig. 16) indicates that intraseasonal AAM fluctuations are strongest when the NEP and NEA centers oscillate in phase, with high (low) zonal wind speeds associated with low (high) 500 mb height

anomalies over both centers. The 300-day modulation in the strength of the model's AAM oscillation noted by MGD (their Fig. 7) arises from interference between the slighly differing frequencies of the NEP and NEA centers (44.5 and 52,5 days, respectively; compare Penland et al. 1991).

Pointwise correlations of the global 500 mb height field with the leading PCs of the NH extratropical 500 mb height field were used to investigate extratropical-tropical teleconnections in the model. Correlation patterns of the unfiltered heights with PCs 1 and 3 showed a characteristic SW-NE tilt, indicative of equatorward energy propagation (Liebmann and Hartmann 1984), while correlations with PC 2 (which did not exhibit strong intraseasonal variations) lacked this feature. In particular, a strong resemblance was noted between the 500 mb correlation pattern leading PC 1 by three days (Fig. 12b) and the "NA" burst documented by Murakami (1988), and between the 500 mb correlation pattern with PC 3 (Fig, 14c) and the "positive Atlantic phase" documented by Weickmann et al. (1985). Since both of these observed patterns are derived from composites related to the MJ oscillation, which is lacking in this version of the model, our results underscore the potential role of extratropical processes in the dynamics of the global intraseasonal oscillation, as suggested by several observational studies (e.g., Liebmann and Hartmann 1984; Lau and Phillips 1986; Murakami 1988; Hsu et al. 1990; Ghil and Mo 1991a,b).

No significant intraseasonal periodicity was found for the zonally-averaged cumulus convection in the tropics during the standard-topography experiment by MGD (their Fig. 16; see also Marcus 1990). An analysis of cumulus convection in 240x25° latitude-longitude boxes located along the equator from the western Indian ocean (WIO) to the dateline — where the OLR signature of the MJ oscillation is the strongest — shows, however, localized activity in both the 36--60 and 16-24 day bands (see Fig. 21). In particular, cumulus precipitation in the WIO (referred to as WIOCP in the main text) has a significant peak at 39 days, which is statistically indistinguishable from the period of the AAM oscillation in the NH extratropics (MGD, Fig. 5). Since the fastest growth rate for

intraseasonal convective disturbances is observed in the WIO (Rui and Wang 1990), it is likely that the intraseasonal periodicity found in WIOCP represents an "incipient" MJ oscillation in this version of the model, a version which fails to simulate the subsequent eastward propagation of sustained convective activity associated with the observed MJ oscillation, Higher-frequency variations seen at periods of 20 and 16.5 days over the Martime Continent and New Guinea, respectively, may be related either to 20-25 and 16-17 day modes found in the tropics (e.g. Ghil and Mo 1991a) or to unrealistically high frequencies associated with the excessively deep cumulus heating profiles found in this and several other GCMs. An improved cumulus scheme with convective downdraft parameterization (Cheng and Arakawa 1991, 1993), currently under development, is expected to produce a more realistic MJ simulation in the UCLA GCM.

b. Discussion

What is the source of the "incipient" MJ oscillation found in the standard-topography model? Since the version of the UCLA GCM used in this study lacks a fully-developed MJ oscillation in the tropics, it appears unlikely that waves propagating eastward around the equator could be the source of the intraseasonal periodicity, as proposed in several studies of the MJ oscillation (e.g., Lorenc 1984; Knutson and Weickmann 1987; Lau and Peng 1987). Indeed, WIOCP spectra from all three of the no-mountain runs have their largest power in the 16-24 day band (Fig. 23), while spectra for three 315-day segments of the standard-topography run, chosen to have approximately the same length as the average duration of the no-mountain runs, all show WIOCP peaks at periods near 40 days. Thus it appears likely that the WIOCP oscillation arises from remote effects of the same topographic instability mechanism found by MGD to generate the NH extratropical AAM oscillation, with approximately the same period, in the standard-topography experiment.

Remote forcing of intraseasonal cumulus activity in the. WIO can be induced by Rossby wave trains propagating from the subtropics, as found by Hsu et al. (1990) in a case study of oscillations during the winter of 985-86. They showed that a strong episode

of convection was triggered by the arrival of a region of ascent associated with a wave train consisting of NE-SW oriented anomalies, extending southeastward from the Atlantic across the Mediterranean and north Africa to the WIO (their Fig. 6). Weickmann et al. (1985) found that a similar wave train (their Fig. 9d) tends to precede the beginning of a new cycle of MJ convection in the Indian Ocean. These results are consistent with the findings of Liebmann and Hartmann (1984), who showed that 500 mb height anomalies with a NE-SW tilt are correlated with equatorward wave-energy propagation and the subsequent enhancement of convective activity to the southeast.

These observed features bear a strong qualitative resemblance to EOF 3 of the NH extratropical 500 mb height field in the model (Fig. 8c), and to the correlation of the global 500 mb height field with PC 3 (i.e., the time-varying amplitude of EOF 3 — see Fig. 14c). Lagged correlations of the 500 mb height field with PC 3 (Figs. 14d,e) show a wave train propagating southeastward towards the Indian Ocean; significant correlations associated with the wave train do not actually reach the WIO, however, and no significant coherence is found in the model between intraseasonal variations in WIOCP and PC 3 (not shown). While the extratropical oscillation in the GCM produces wave trains similar to those identified by Hsu et al. (1990) and Weickmann et al. (1985) as precursors to the tropical MJ oscillation, therefore, these Atlantic-sector teleconnections are not directly linked to cumulus activity over the WIO in this version of the model.

In the Pacific sector, correlations of PC 1 with the global 500 mb height field at lags of -3 days (Fig. 12b) and +3 days (Fig. 12d) bear a strong resemblance to the "NA" and "NP" surges, respectively, derived by Murakami (1988) from 30-60 day filtered composites of the 850 mb streamfunction during northern winter. Both the GCM and the observed NA teleconnection patterns have a pronounced NW-SE tilt, extending from Siberia along the western Tibetan Plateau to the Arabian Sea and the WIO. Cumulus precipitation in the model WIO shows significant coherence with PC 1 in the intraseasonal band (Fig. 22), and reaches its maximum intensity at a lag of three days after the passage

through the WIO of a trough associated with EOF 1 of the NH extratropical 500 mb height field (Fig. 12b). The observed NA composites were keyed to minimum OLR in the eastern Indian Ocean, however, and are most strongly correlated with intraseasonal convection in the western Pacific at a lag of 15 days. While the mechanism for this remote effect is not clear, the subsequent appearance of convection over the western Pacific may be triggered by NP surges, which tend to follow the NA pattern at about the same lag (Murakami 1988), In the GCM, however, the NP pattern (Fig. 12d) follows the NA pattern at a lag of only 6 days, and does not show significant coherence with cumulus precipitation over the western Pacific,

Some differences are found, therefore, between simulated and observed features of tropical-extratropical interaction in the intraseasonal band during NH winter. The lack of an MJ oscillation in this version of the model renders the similarities more noteworthy, however, and strengthens the working hypothesis that intraseasonal variability originating in the extratropics may play a key role in modulating the equatorward flux of wave-energy, and lead to the initiation of nearly periodic flare-ups of convective activity in the tropics (Liebmann and Hartmann 1984; Murakami 1988; Hsu et al. 1990), In order to verify this hypothesis, further studies will be needed to determine the nature and origin of the wave-energy fluxes involved, and the specific mechanisms by which they influence tropical convective activity on intraseasonal time scales.

Acknowledgments. It is a pleasure to acknowledge discussions with A. Arakawa and C. R. Mechoso on the UCLA GCM. J. Spahr helped with the runs and extracting the requisite output fields. This work was supported at UCLA by NASA grant NAG5-3 17, and by an NSF Special Creativity Award to M.G. The work of S.L.M. and J.O.D. is the result of one phase of research carried out at the Jet Propulsion Laboratory, California Institute of Technology, sponsored by the National Aeronautics and Space Administration,

References

Anderson, J. A., and R. D. Rosen, 1983: The latitude-height structure of 40-50 day variations in atmospheric angular momentum. *J. Atmos. Sci.,* 40, 1583-1591.

Barnston, A. G., and R. E. Livezey, 1987: Classification, seasonality and persistence of low frequency atmospheric circulation patterns. Mon. *Wea. Rev.,* 115, 1083-1126.

Benedict, W. L., and R. L. Haney, 1988: Contribution of tropical winds to subseasonal fluctuations in atmospheric angular momentum and length of day. *J. Geophys. Res.,* 93, 15973-15978.

Bernardet, P., A. Butet, M. Deque, M. Ghil, and R. L. Pfeffer, 1990: Low-frequency oscillations in a rotating annulus with topography. *J. Atmos. Sci., 47, 3023-3043.*

Boer, J. G., 1990: Earth-atmosphere exchange of angular momentum simulated in a general circulation model and implications for the length of day. *J. Geophys. Res.,* 95, 5511-5531.

Branstator, G., 1987: A striking example of the atmosphere's leading traveling pattern. *J. Atmos. Sci., 44, 2310-2323.*

Chang, C.-P., and K. M. Lau, 1982: Short-term planetary-scale interactions over the tropics and midlatitudes during northern winter. Part I: Contrasts between active and inactive periods. *Mon. Wea. Rev.,* 110, 933-946.

Cheng, M. D., and A. Arakawa, 1991: Inclusion of rainwater budget and convective downdrafts in a cumulus parameterization. *Ninth Conference on Numerical Weather Prediction,* Amer. Meteor. Sot., Boston, Mass.

Cheng, M. D., and A. Arakawa, 1993: A cumulus pararneterization with rainwater budget and convective downdraft. *Twentieth Conference on Hurricane and Tropical Meteorology,* Amer. Meteor. Sot., Boston, Mass.

Dickey, J. O., M. Ghil, and S. L. Marcus, 1991: Extratropical aspects of the 40-50 day oscillation in length-of-day and atmospheric angular momentum. *J. Geophys. Res.*, 96, 22643-22658,

Fultz, D., R. R. Long, G. V. Owens, W. Bohan, R. Kaylor and J. Weil, 1959: Studies of Thermal Convection in a Rotating Cylinder with Some Implications for Large-Scale Atmospheric Motions. *Meteorol. Monogr.*, *4*, American Meteorological Society, Boston, Mass., pp. 1-104.

Ghil, M., 1987: Dynamics, statistics and predictability of planetary flow regimes. In *Irreversible Phenomena and Dynamical Systems Analysis in Geosciences, C.* Nicolis and G. Nicolis (eds.), D. Reidel, Dordrecht, pp. 241-283.

Ghil, M., 1988: Nonlinear approaches to low-frequency variability. In *Dynamics of Low-Frequency Phenomena in the Atmosphere, G.* Branstator, R. Madden and J. Tribbia, (eds.), NCAR, Boulder, CO 80307, pp. 603-714.

Ghil, M., and S. Childress, 1987: *Topics in Geophysical Fluid Dynamics: Atmospheric Dynamics, Dynamo Theory, and Climate Dynamics.* Springer-Verlag, Berlin/New York/Tokyo, 485 pp.

Ghil, M., and K. Mo, 1991a: Intraseasonal oscillations in the global atmosphere, Part I, Northern hemisphere and tropics, *J. Atmos. Sci.*, 48,752-779.

Ghil, M., and K. Mo, 1991b: Intraseasonal oscillations in the global atmosphere, Part II, Southern hemisphere, *J. Atmos. Sci.*, 48, 780-790.

Gutzler, D. S., and R. A, Madden, 1993: Seasonal variations of the 40-50 day oscillation in atmospheric angular momentum. *J. Atmos. Sci.*, 50, 850-860,

Hartmann, D, L., and M. L. Michelsen, 1989: Intraseasonal periodicities in Indian rainfall. *J. Atmos. Sci.*, 46, 2838-2862.

Hartmann, D. L., M. L. Michelsen, and S. A, Klein, 1992: Seasonal variations of tropical intraseasonal oscillations: a 20-25 day oscillation in the western Pacific. *J, Atrnos. Sci.*, 49, 1277-1289.

Hayashi, Y.-Y., and A. Sumi, 1986: The 30-40 day oscillations simulated in an "aqua planet" model. *J. Meteorol. Sot. Jpn.*, *64, 451-467.*

Hide, R., 1977: Experiments with rotating fluids. *Quart. J. Roy. Meteorol. Sot.,* 103, 1-28.

Hide, R., and J. O. Dickey, 1991: Earth's variable rotation. *Science,* 253,629-637.

Hsu, H.-H., B. J. Hoskins, and F.-F. Jin, 1990: The 1985/86 intraseasonal oscillation and the role of the extratropics. *J. Atmos. Sci.*, 47, 823-839.

Jin, F. F., and M. Ghil, 1990: Intraseasonal oscillations in the extratropics: Hopf bifurcation and topographic instabilities. *J. Atmos. Sci.,* 47, 823-839.

Keppenne, C. L., and M. Ghil, 1994: Intraseasonal oscillations in a two-layer model. *J. Atmos. Sci.*, sub judice.

Knutson, T. R., and K.. M. Weickmann, 1987: 30–60 day atmospheric oscillations: composite life cycles of convection and circulation anomalies. Mon. *Wea. Rev.,* 115, 1407-1436.

Krishnamurti, T. N., and Gadgil, S., 1985: On the structure of the 30 to 50 day mode over the globe during FGGE. *Tellus*, *37A, 336-360.*

Kushnir, Y., 1987: Retrograding wintertime low-frequency disturbances over the North Pacific Ocean. *J. Atmos. Sci.*, 44, 2727-2742.

Lau, K.-M., and L. Peng, 1987: Origin of low-frequency (intraseasonal) oscillations in the tropical atmosphere. Part I: Basic theory. *J. Atmos. Sci.*, 44,950-972.

Lau, K.-M., and T. J, Phillips, 1986: Coherent fluctuation of extratropical geopotential height and tropical convection in intraseasonal time scales. *J. Atmos. Sci.*, 43, 1164-1181.

Lau, K.-M., I. S. Kang and P. J. Sheu, 1989: Principal modes of intraseasonal variation in atmospheric angular momentum and tropical convection. *J. Geophys. Res,* **94**, 6319-6332.

Lau, N. C., and K.-M. Lau, 1986: Structure and propagation of intraseasonal oscillations appearing in a GFDL GCM, *J. Atmos. Sci.*, *43, 2023-2047.*

Legras, B., and M. Ghil, 1985: Persistent anomalies, blocking, and variations in atmospheric predictability y. *J. Atmos. Sci.*, 42, 433-471.

Liebmann, B., and D, L. Hartmann, 1984: An observational study of tropical-midlatitude interaction on intraseasonal time scales during winter. *J. Atmos. Sci.*, 41, 3333-3350.

Lorenc, A. C., 1984: The evolution of planetary-scale 200mb divergent flow during the FGGE year. *Quart. J. Roy. Meteor. Sot.*, 110, 427-441.

Lorenz, E. N., 1967: *The Nature and Theory of the General Circulation of the Atmosphere.* World Meteorological Organization, Geneva, Switzerland, 161 pp.

Madden, R. A., 1979: Observations of large-scale traveling Rossby waves. *Rev. Geophys. Space Phys.*, *17, 1935-1949.*

Madden, R. A., and P. R. Julian, 1971: Detection of a 40-50 day oscillation in the zonal wind in the tropical Pacific. *J. Atmos. Sci., 28, 702-708.*

Madden, R. A., and P. R, Julian, 1972: Description of global-scale circulation cells in the tropics with a 40-50 day period. *J, Atmos. Sci., 29,* 1109-1123.

Madden, R. A., and P. R. Julian, 1994: Observations of the 40-50 day tropical oscillation - a review. NCAR/0401/92-29.

Magaña, V., 1993: The 40- and 50-day oscillations in atmospheric angular momentum at various latitudes. *J, Geophys. Res., 98,* 10441-10450.

Magaña, V., and M. Yanai, 1991: Tropical-midlatitude interaction on the time scale of 30 to 60 days during the northern summer of 1979. *J. Climate, 4, 180-201.*

Marcus, S. L., 1990: Intraseasonal oscillations in the Earth-atmosphere system, Ph. D. Thesis, University of California, Los Angeles, 184 pp.

Marcus, S. L., M. Ghil, and J. O. Dickey, 1994: The extratropical 40-day oscillation in the UCLA general circulation model. Part I: Atmospheric angular momentum. *J. Atmos. Sci.,* 51, 1431-1446.

Mechoso, C. R., A. Kitoh, S. Moorthi, and A. Arakawa, 1987: Numerical simulations of the atmospheric response to a sea-surface temperature anomaly over the equatorial eastern Pacific ocean. *Mon. Wea. Rev.,* 115, 2936-2956.

Mo, K. C., and M. Ghil, 1987: Statistics and dynamics of persistent anomalies. *J. Atmos. Sci., 44, 877-901.*

Murakami, T., 1988: Intraseasonal atmospheric teleconnection patterns during the northern hemisphere winter. *J. Climate,* 1, 117-131.

Namias, J., 1950: The index cycle and its role in the general circulation. *J. Meteorol.,* 7, 130-139.

Neelin, J. D., I. M. Held, and K. H. Cook, 1987: Evaporation-wind feedback and low-frequency variability in the tropical atmosphere. *J. Atmos. Sci., 44,2341-2348,*

Penland, C., M. Ghil, and K.. M. Weickmann, 1991: Adaptive filtering and maximum entropy spectra with application to changes in atmospheric angular momentum, *J. Geophys. Res.,* 96, 22659-22671,

Pitcher, E. J., and J. E, Geisler, 1987: The 40-to 50-day oscillation in a perpetual January simulation with a general circulation model. *J. Geophys. Res.,* 92, 11971-11978,

Rui, H., and B. Wang, 1990: Development characteristics and dynamic structure of tropical intraseasonal convection anomalies. *J. Atmos. Sci.,* 47, 357-379.

Simmons, A. J., J. M. Wallace, and G. W. Branstator, 1983: Barotropic wave propagation and instability and atmospheric teleconnection patterns. *J. Atmos. Sci.,* 40, 1363-1392, 1983.

Strong, C. M., 1994: Intraseasonal variability and extended-range prediction in the Northern Hemisphere extratropics. Ph. D. Thesis, University of California, Los Angeles, 161 pp.

Strong, C. M., F.-F. Jin, and M. Ghil, 1993: Intraseasonal variability in a barotropic model with seasonal forcing. *J. Atmos. Sci., 50, 2965-2986.*

Sumathipala, W. L., and T. Murakami, 1988: Intraseasonal fluctuations in low-level meridional winds over the south China Sea and the western Pacific and monsoonal convection over Indonesia and northern Australia. *Tellus, 40A, 205-129.*

Tokioka, T., K. Yamazaki, A. Kitoh, and T. Ose, 1988: The equatorial 30-60 day oscillation and the Arakawa-Schubert penetrative cumulus parametization, *J. Met. Soc. Japan, 66, 883-901.*

Trenberth, K. E., and K. C. Mo, 1985: Blocking in the Southern Hemisphere. *Men, Wea. Rev.,* 113, 3-21.

Tribbia, J. J., and M. Ghil, 1990: Forced zonal flow over topography and the 30----60 day oscillation in atmospheric angular momentum. NCAR 0501/89-5, National Center for Atmospheric Research, Boulder, Colorado, 26 pp.

Weickmann, K. M., G. R. Lussky, and J, E. Kutzbach, 1985: Intraseasonal (30-60 day) fluctuations of outgoing longwave radiation and 250 mb streamfunction during northern winter. *Mon. Wea. Rev., 113, 941-961.*

Weickmann, K. M., S. J. S. Khalsa, and J. Eischeid, 1992: The atmospheric angular momentum cycle during the tropical Madden-Julian Oscillation, *Mon. Wea. Rev., 120, 2252-2263.*

Figure Captions

Fig. 1. Mean 500 mb height field. (a) Standard-topography run; (b) last 360 days of the longest no-mountain run. A 50° overlap in the longitude scale is used here and in all subsequent maps to improve legibility of patterns cut off by the maps' right and left margins.

Fig. 2. (a) Root-mean-square (rms) departure of 500 mb height from its mean value during the standard-topography run; (b) as in (a), for the 500 mb height filtered in the 36—60 day band at each grid point. (c) Power spectrum of the daily rms change of the 500 mb height field on an equal-area grid for the NH extratropics (20°N-90°N). The bandwidth on this and all subsequent spectra having logarithmic abscissa pertains only to the frequency at which it is plotted.

Fig. 3. Ratio of 36--60 day filtered to the unfiltered rms height departure at 500 mb for the standard-topography run. Contour interval is 0.04, starting at 0,20. Note the pronounced southwest-northeast tilt of the intraseasonal variance maxima in the NH extratropics.

Fig. 4. Composite 500 mb maps. (a) For days on which the 36—60 day NH extratropical AAM exceeded 1.5 time its rms value during the standard-topography run; maps for days with a negative (positive) anomaly were added with a positive (negative) sign. (b) Constructed from maps taken 12 days earlier than those included in (a). Contour interval is 20 m; solid (dashed) lines show positive (negative) anomalies in this and subsequent figures.

Fig. 5. Composite 500 mb anomalies from days 94-225 of the standard-topography run, corresponding to the (a) maximum, (b) decreasing, (c) minimum, and (d) increasing phase of the 36-60 day AAM cycle in the NH extratropics (20°N—90°N).

Fig. 6. As in Fig. 5, for the full 500 mb height field from days 94-225 of the standard-topography run.

Fig, 7. Variance fraction carried by the first 20 EOFS for the unfiltered (solid) and 36--60 day filtered (dotted) 500 mb height fields. Note the greater efficiency of the EOF decomposition for the filtered case.

Fig, 8. First three EOFS (panels a-c) for the. unfiltered 500 mb height fields for the NH extratropics from the standard-topography run, computed on a reduced grid of 445 points.

Fig. 9. Power spectra for the leading three PCs of the unfiltered 500 rnb height fields for the NH extratropics from the standard-topography run. The period on this and all subsequent spectra ranges from two weeks (right margin) to ten weeks (left margin), (a) PC 1 (solid) and PC 3 (dashed); the 44.5-day peak for PC 1 is significant at the 90% level with respect to an autoregressive process of order one (AR1: not shown), while the 52.5-day peak for PC 3 is significant at the 95% level, (b) PC 2 ; note difference in the vertical scale.

Fig. 10. Phase relationship between PCs 1 and 3 of the unfiltered 500 mb height field from the NH extratropics. (a) Squared coherence; highly significant peaks (> 99%) are found at periods of 39 and 15.5 days. (b) Phase difference; over the intraseasonal (36-60 day) band, PC 1 tends to lead PC 3 by about 6 days.

Fig. 11. Squared coherence of (a) PC 1, (b) PC 2, and (c) PC 3 with the NH extratropical AAM from the standard-topography run.

Fig. 12. Correlation coefficient of PC 1 (defined in the NH extratropics) with the global 500 mb height field. The lag for the 500 mb height field increases by three days per frame, starting from -6 days for frame (a). Solid (dashed) contours begin at 0.16 (—0. 16), representing correlations significant at approximately the 95% level (see text), and increase (decrease) in steps of 0.08. The sign of the PC was reversed before plotting the correlations, in order to emphasize tropical teleconnections by solid contours.

Fig, 13. As in Fig. 12, for PC 2.

Fig. 14. As in Fig. 12, for PC 3.

Fig. 15. First three EOFS (panels a-c) for the 36-60 day filtered 500 mb height fields from the NH extratropics for the standard-topography run.

Fig. 16. Cross-correlations between the 36-60 day filtered AAM from the NH extratropics and the two leading PCFS for the standard-topography run,

Fig. 17. Correlation coefficient of PCF 1 with the 36—60 day filtered 500 mb height field. The lag for the 500 mb height field increases by three days per frame, starting from —6 days for frame (a). Solid (dashed) contours begin at 0.40 (-0.40) and increase (decrease) in steps of 0.10. The sign of the PCFS was reversed before plotting the correlation, in order to emphasize tropical features.

Fig. 18. As in Fig. 17, for PCF 2.

Fig. 19. As in Fig, 17, for PCF 3.

Fig. 20. Cross-correlation between PCF 1 and the average 500 mb height field in the tropics (200S—200N) filtered in the 36—60 day band.

Fig. 21. Spectra of cumulus precipitation from the model's standard-topography run, computed for six separate regions (panels a to f), extending from 12°S to 12°N over the longitudes indicated. The bandwidth is the same for all panels, but is plotted at different ordinates for ease of viewing, The peak at 39 days in panel (a) is significant at the 95% level with respect to an AR 1 process; so are the peaks at 20 days in panel (c) and at 16.5 days in panel (d).

Fig. 22. Coherence squared of WIOCP (cumulus precipitation in the western Indian ocean) with PC 1 of the 500 mb height field from the NH extratropics. The phases of WIOCP and PC 1 (not shown) are statistically indistinguishable in the intraseasonal band.

Fig. 23. Spectra of cumulus precipitation in the western Indian Ocean (latitude 120S to 12°N, longitude 550E to 75°E). Panels (a) to (c) show results from the three no-mountain experiments; the first 40 days were dropped from each run to eliminate transients. Panels (d) to (f) show results from the standard-topography experiment, for three 3 15-day segments separated by 40 days; the length of each segment is approximate] y the same as the

average length of the no-mountain runs. The bandwidth is the same for all panels, but is plotted at different ordinates for ease of viewing.

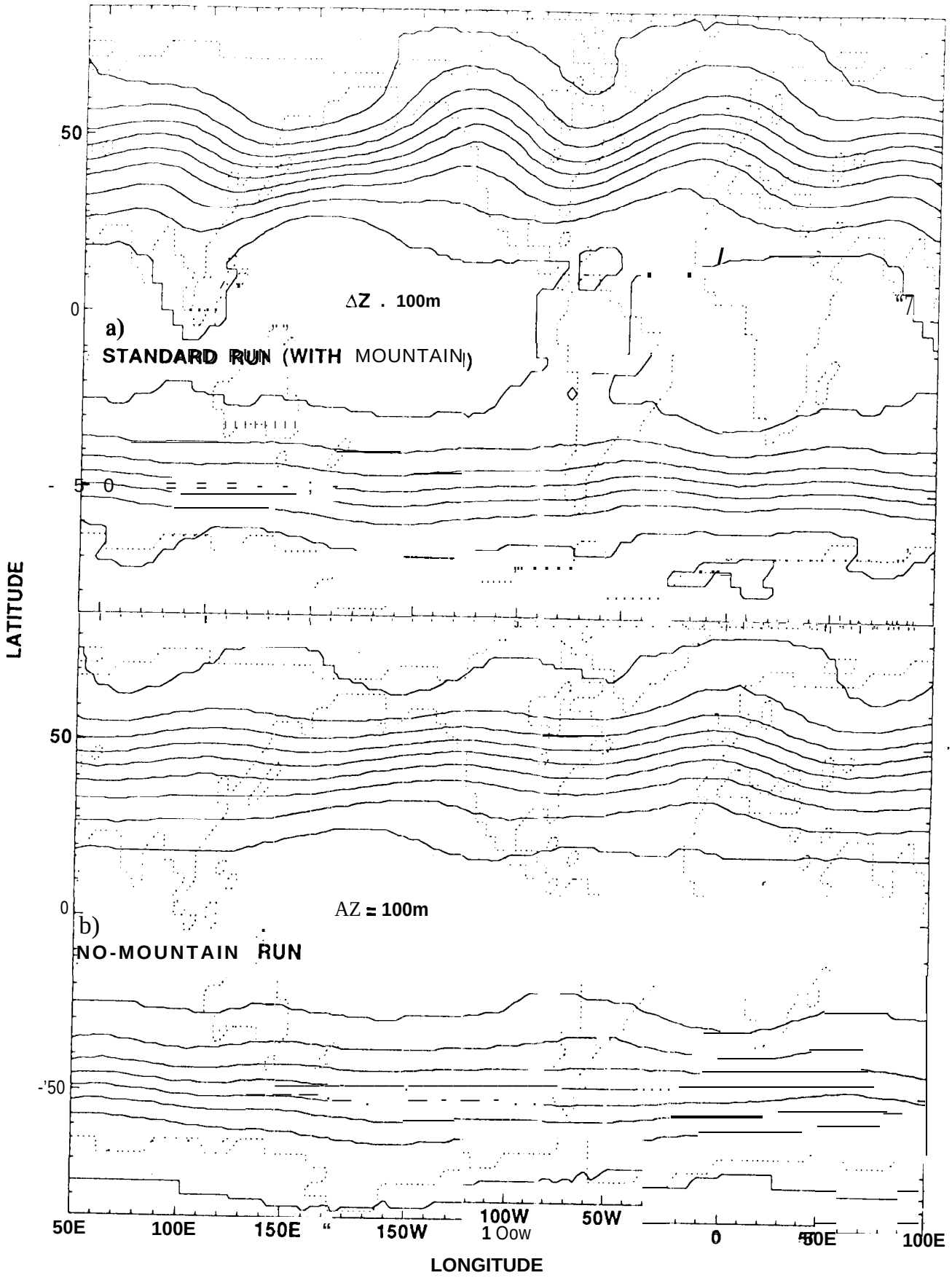
50
0
ΔZ . 100m
a)
STANDARD RUN (WITH MOUNTAIN)
50
0
AZ = 100m
b)
NO-MOUNTAIN RUN
-'50
LATITUDE
50E
100E
150E
150W
100W
1 Oow
50W
0
50E
100E
LONGITUDE

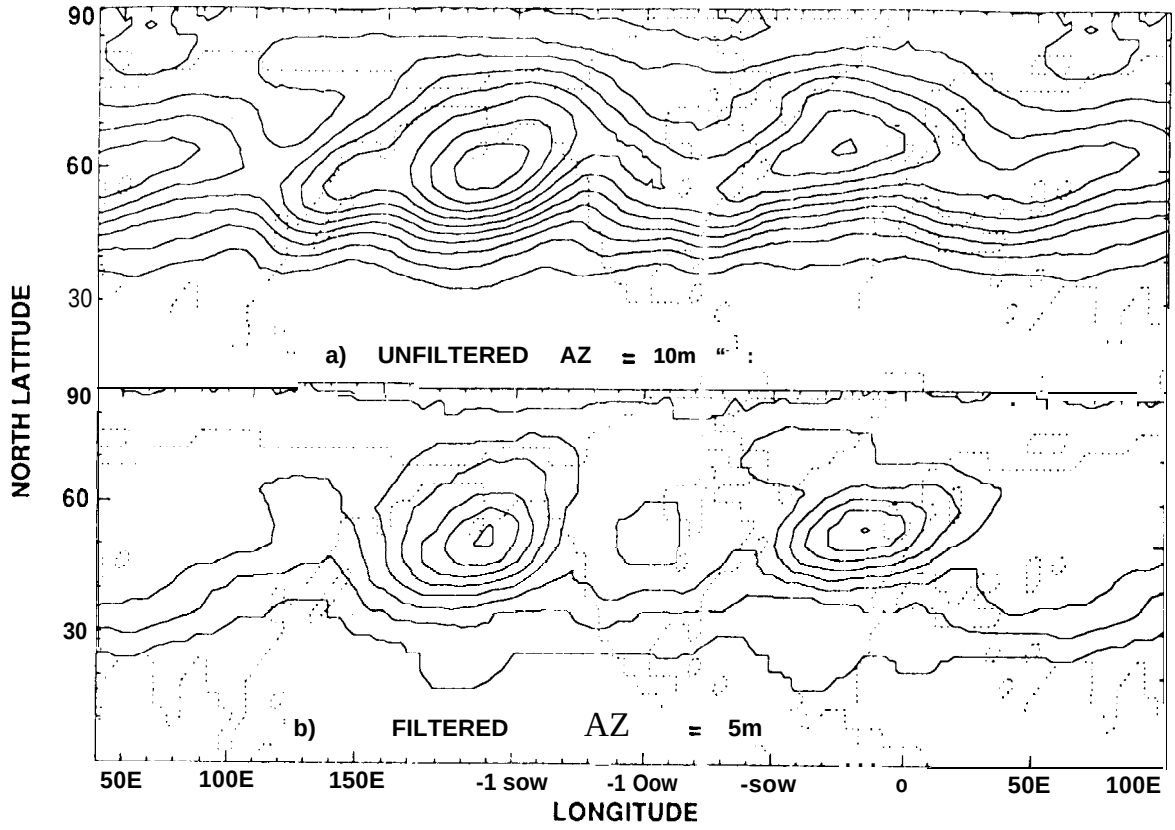
90
60
30
NORTH LATITUDE
a) UNFILTERED AZ = 10m
90
60
30
b) FILTERED AZ = 5m
50E
100E
150E
-1 sow
-1 Oow
-sow
o
50E
100E
LONGITUDE

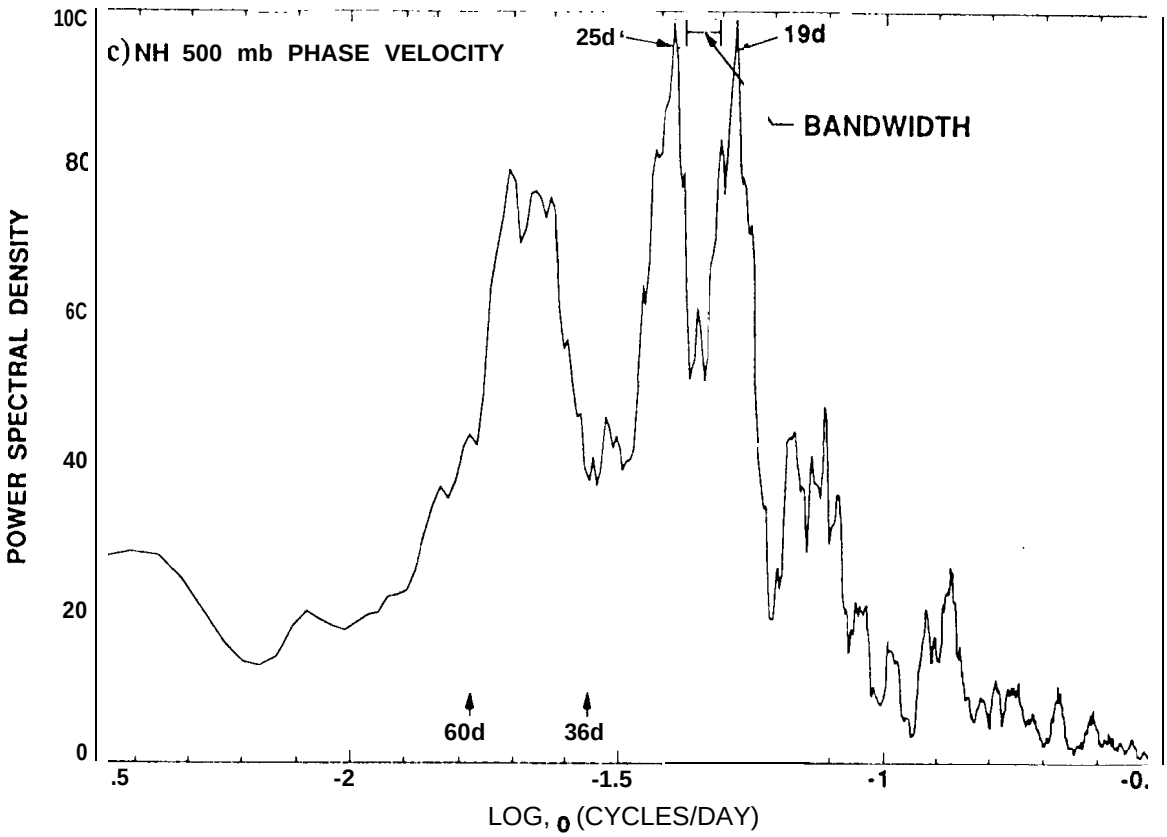
10C
8C
6C
40
20
0
POWER SPECTRAL DENSITY
c) NH 500 mb PHASE VELOCITY
25d
19d
BANDWIDTH
60d
36d
.5
-2
-1.5
-1
-0.
LOG, 0 (CYCLES/DAY)

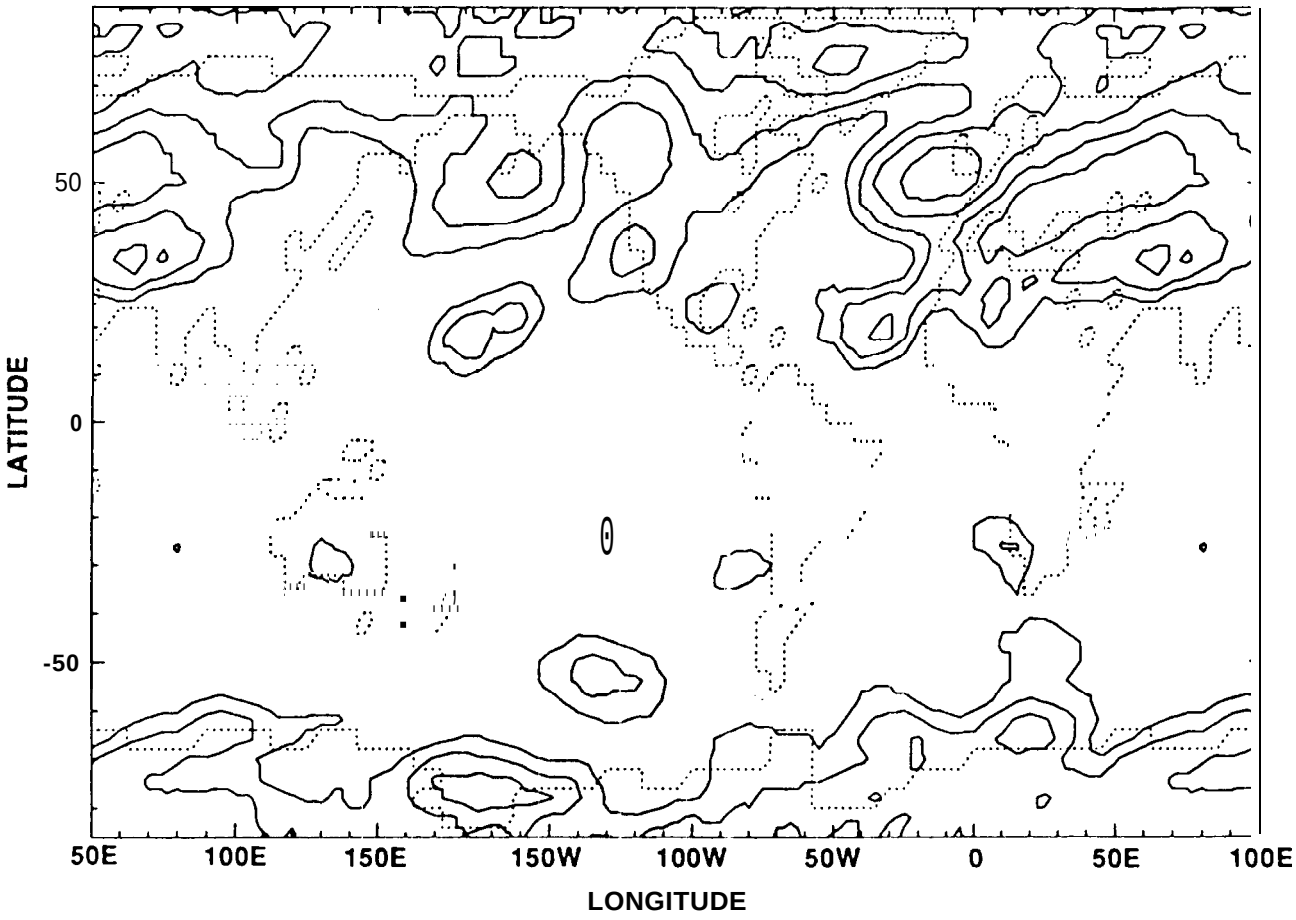
50
0
-50
LATITUDE
50E
100E
150E
150W
100W
50W
0
50E
100E
LONGITUDE

3

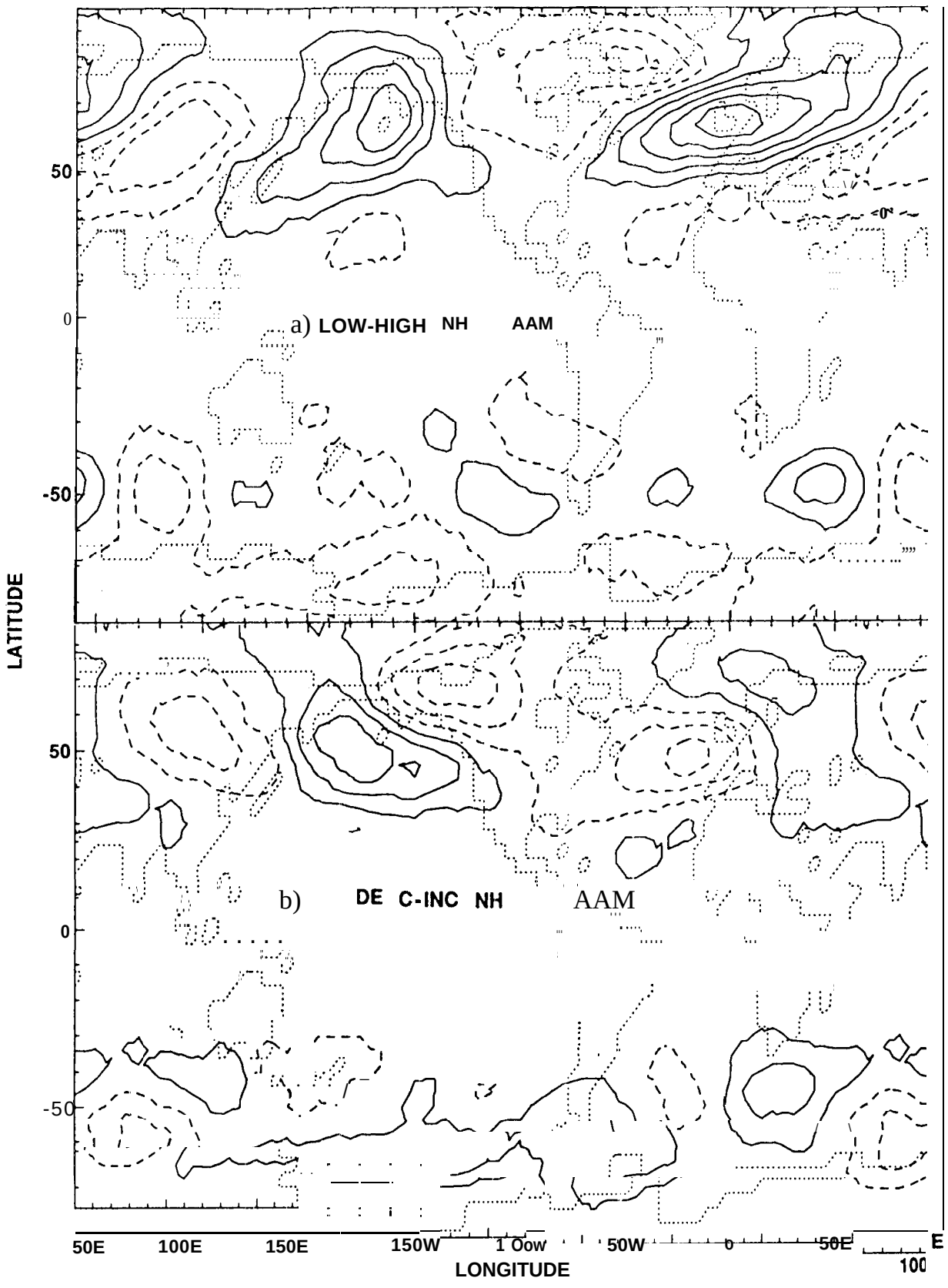
a) LOW-HIGH NH AAM
b) DE C-INC NH AAM
LATITUDE
50
0
-50
50
0
-50
50E
100E
150E
150W
1 Oow
50W
0
50E
E
100
LONGITUDE

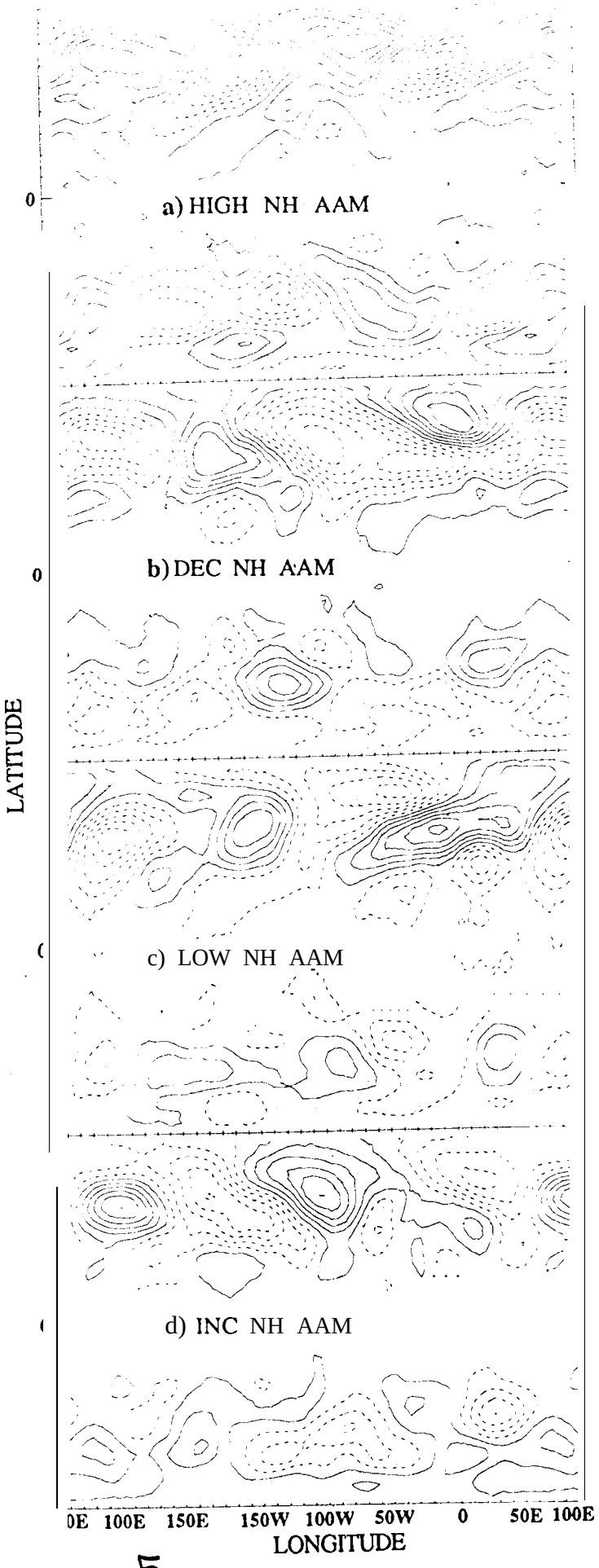
a) HIGH NH AAM
b) DEC NH AAM
c) LOW NH AAM
d) INC NH AAM
0
0
0E 100E 150E 150W 100W 50W 0 50E 100E
LONGITUDE
LATITUDE

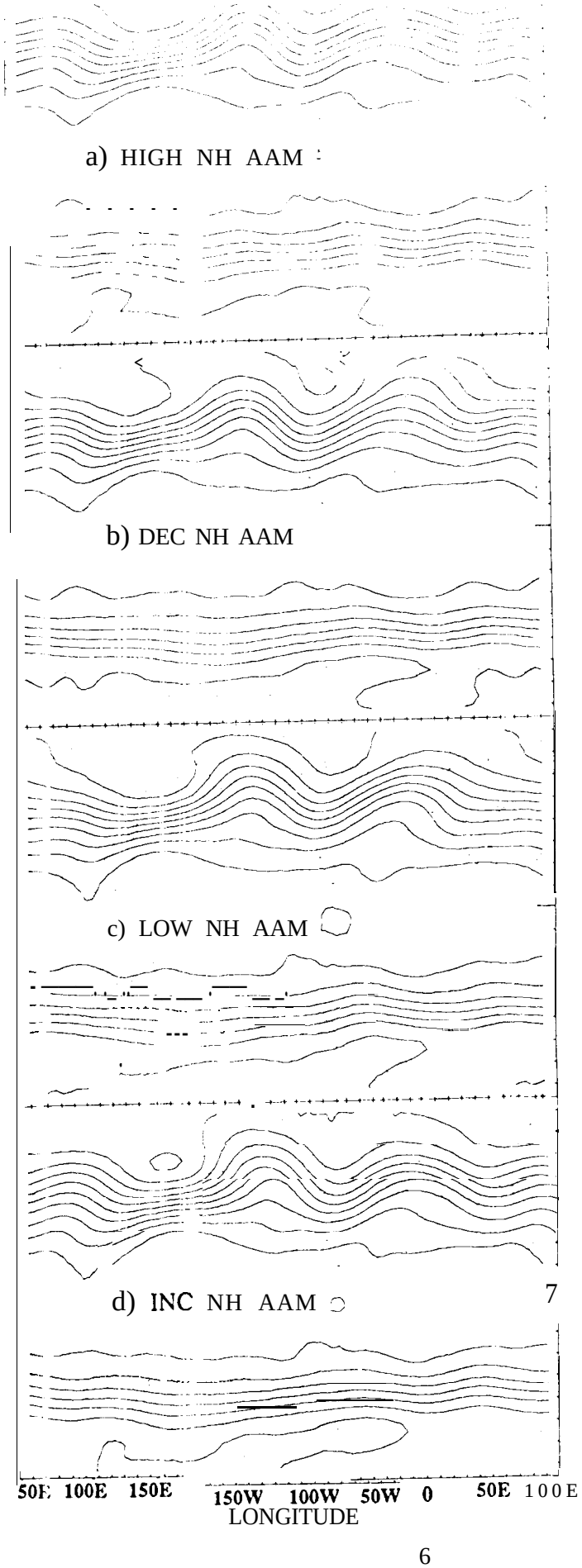
a) HIGH NH AAM
b) DEC NH AAM
c) LOW NH AAM
d) INC NH AAM
50E 100E 150E 150W 100W 50W 0 50E 100E
LONGITUDE

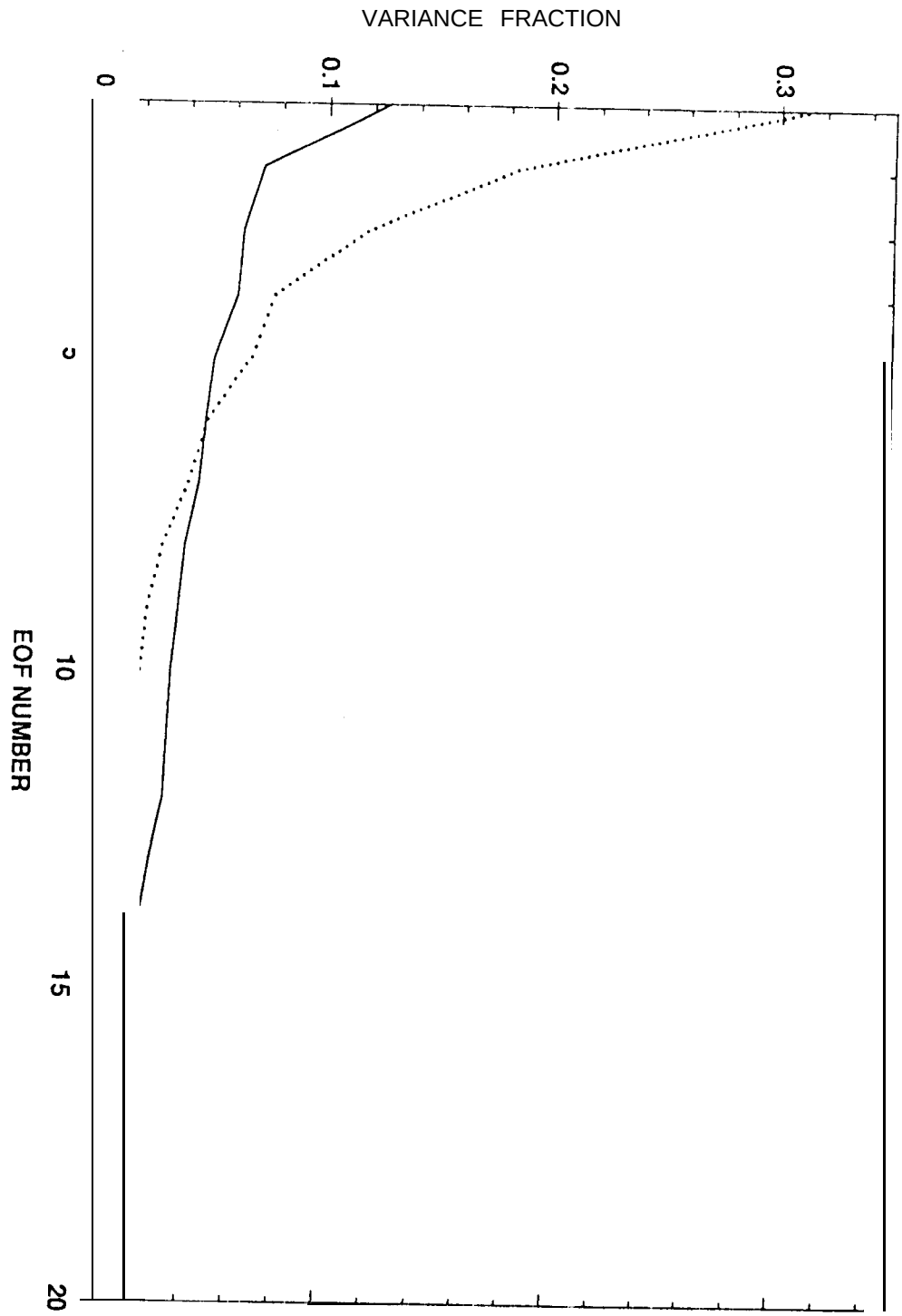
VARIANCE FRACTION
0
0.1
0.2
0.3
5
10
15
20
EOF NUMBER

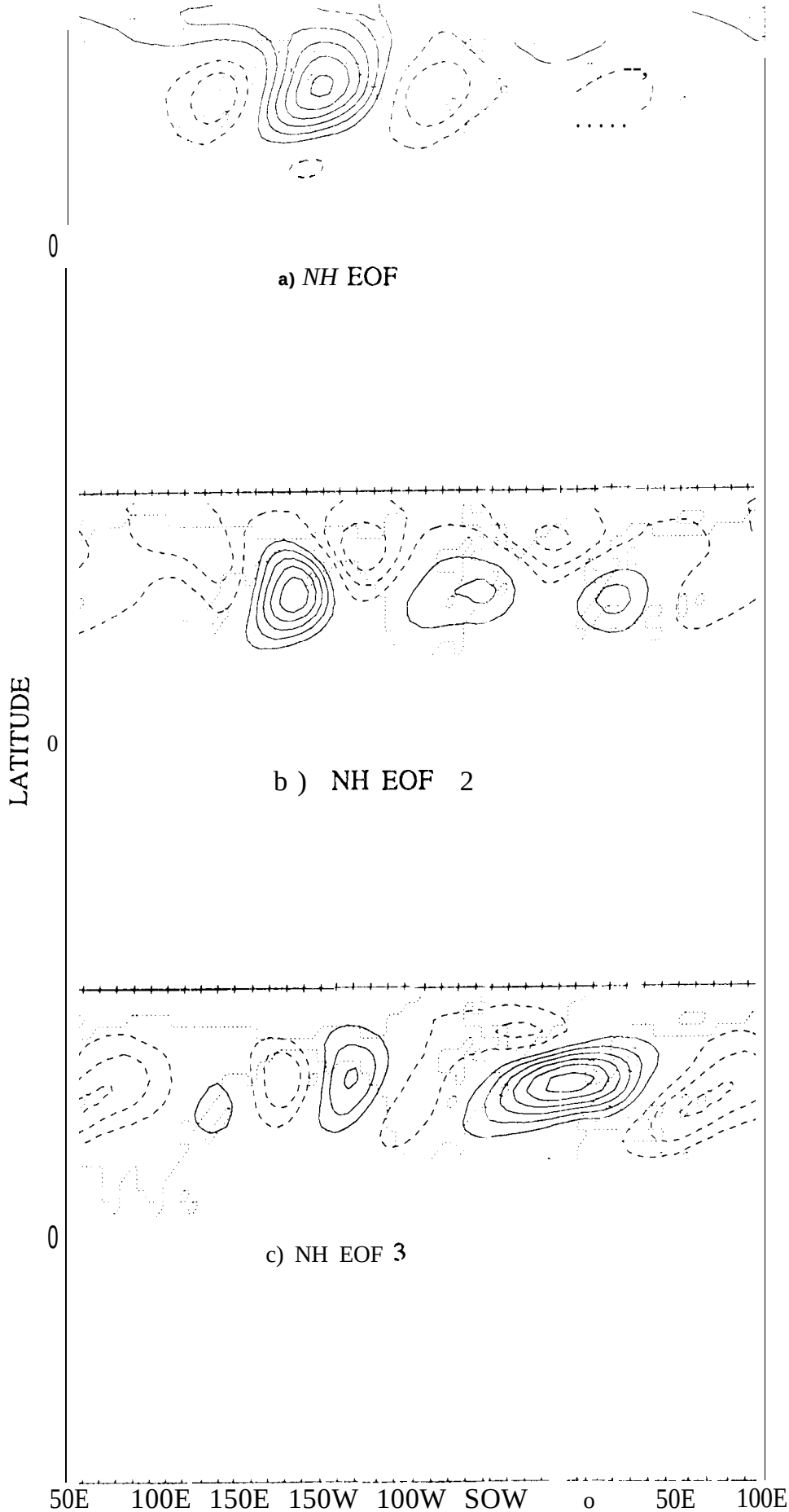
0
a) NH EOF
0
b) NH EOF 2
LATITUDE
0
c) NH EOF 3
50E 100E 150E 150W 100W SOW o 50E 100E
LONGITUDE

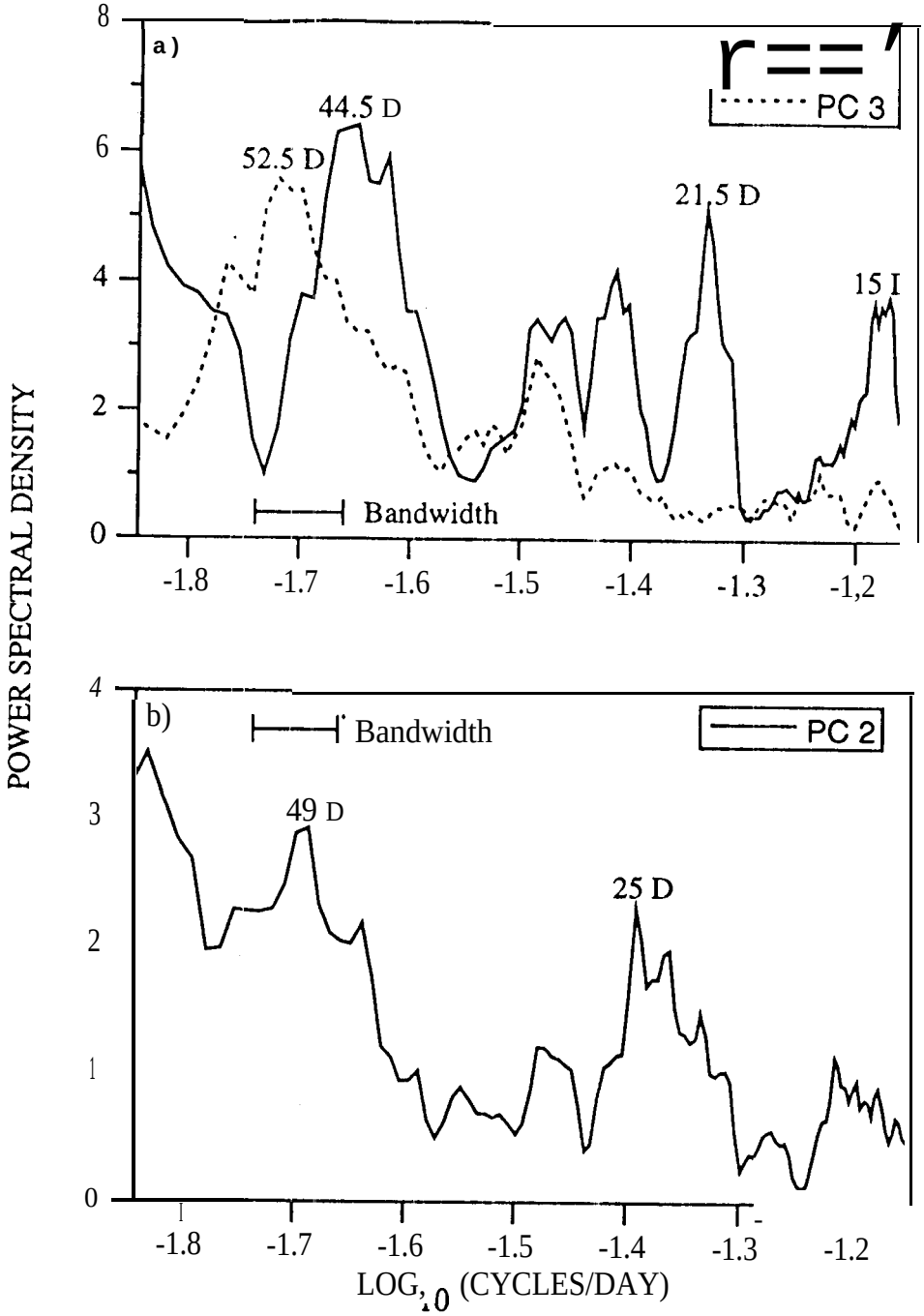
a)
r = ?
PC 3
44.5 D
52.5 D
21.5 D
15 I
Bandwidth
8
6
4
2
0
-1.8
-1.7
-1.6
-1.5
-1.4
-1.3
-1,2
b)
Bandwidth
PC 2
49 D
25 D
4
3
2
1
0
-1.8
-1.7
-1.6
-1.5
-1.4
-1.3
-1.2
POWER SPECTRAL DENSITY
LOG10 (CYCLES/DAY)

9

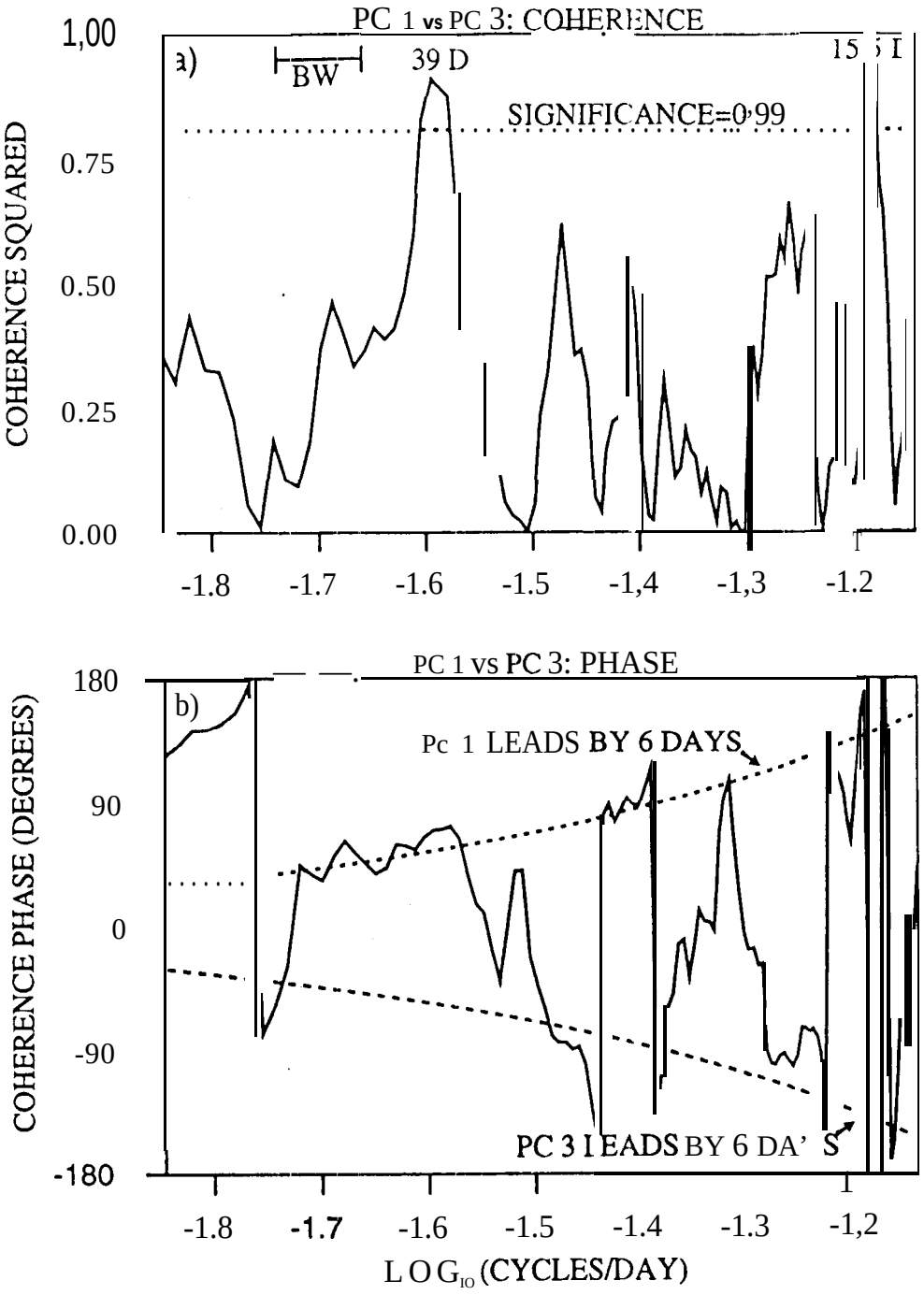
PC 1 vs PC 3: COHERENCE
a)
BW
39 D
SIGNIFICANCE=0.99
COHERENCE SQUARED
1.00
0.75
0.50
0.25
0.00
-1.8
-1.7
-1.6
-1.5
-1,4
-1,3
-1.2
PC 1 vs PC 3: PHASE
b)
Pc 1 LEADS BY 6 DAYS
PC 3 LEADS BY 6 DAYS
COHERENCE PHASE (DEGREES)
180
90
0
-90
-180
-1.8
-1.7
-1.6
-1.5
-1.4
-1.3
-1,2
LOG10 (CYCLES/DAY)

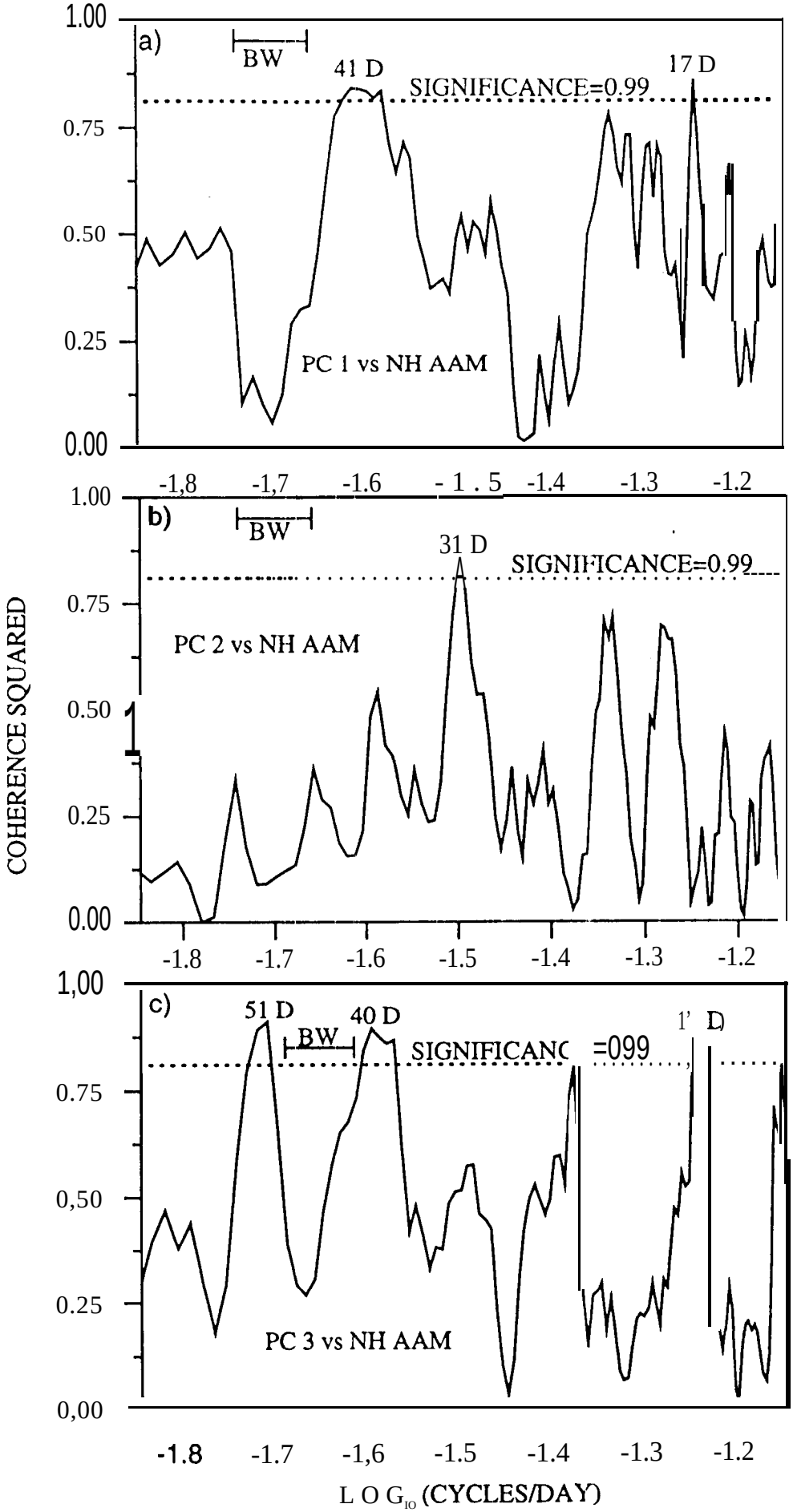
a)
BW
41 D
17 D
SIGNIFICANCE=0.99
PC 1 vs NH AAM
1.00
0.75
0.50
0.25
0.00
-1,8
-1,7
-1.6
- 1 . 5
-1.4
-1.3
-1.2
b)
BW
31 D
SIGNIFICANCE=0.99
PC 2 vs NH AAM
1.00
0.75
0.50
0.25
0.00
-1.8
-1.7
-1.6
-1.5
-1.4
-1.3
-1.2
c)
51 D
40 D
BW
SIGNIFICANC =099
1' D
PC 3 vs NH AAM
1,00
0.75
0,50
0.25
0,00
-1.8
-1.7
-1,6
-1.5
-1.4
-1.3
-1.2
COHERENCE SQUARED
L O G10 (CYCLES/DAY)

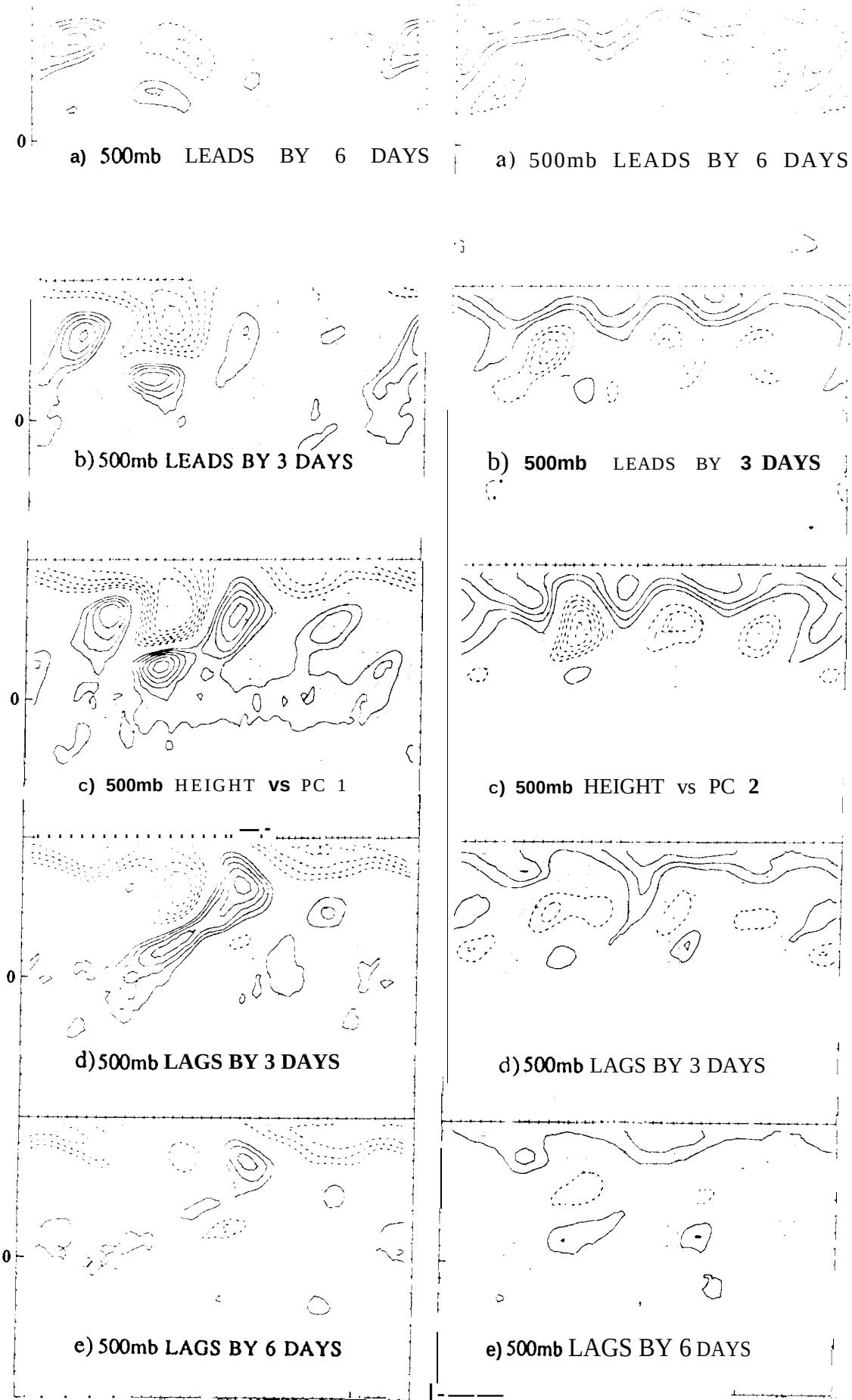
0
a) 500mb LEADS BY 6 DAYS
b) 500mb LEADS BY 3 DAYS
0
c) 500mb HEIGHT vs PC 1
0
d) 500mb LAGS BY 3 DAYS
0
e) 500mb LAGS BY 6 DAYS
LATITUDE
50E 100E 150E 150W 100W 50W 0 50E 100E
LONGITUDE
a) 500mb LEADS BY 6 DAYS
b) 500mb LEADS BY 3 DAYS
c) 500mb HEIGHT vs PC 2
d) 500mb LAGS BY 3 DAYS
e) 500mb LAGS BY 6 DAYS
50E 100E 150E 150W 100W 50W 0 50E 100E
LONGITUDE

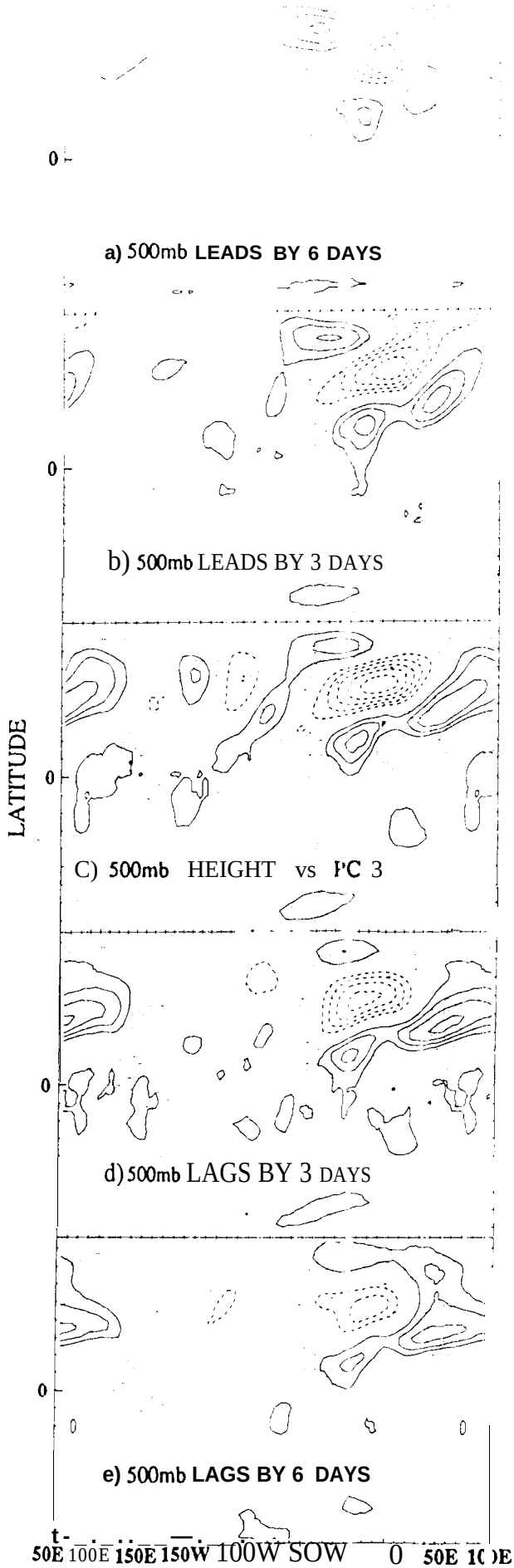
0
a) 500mb LEADS BY 6 DAYS
0
b) 500mb LEADS BY 3 DAYS
LATITUDE
0
C) 500mb HEIGHT vs PC 3
0
d) 500mb LAGS BY 3 DAYS
0
e) 500mb LAGS BY 6 DAYS
50E 100E 150E 150W 100W SOW 0 50E 1C)E
LONGITUDE

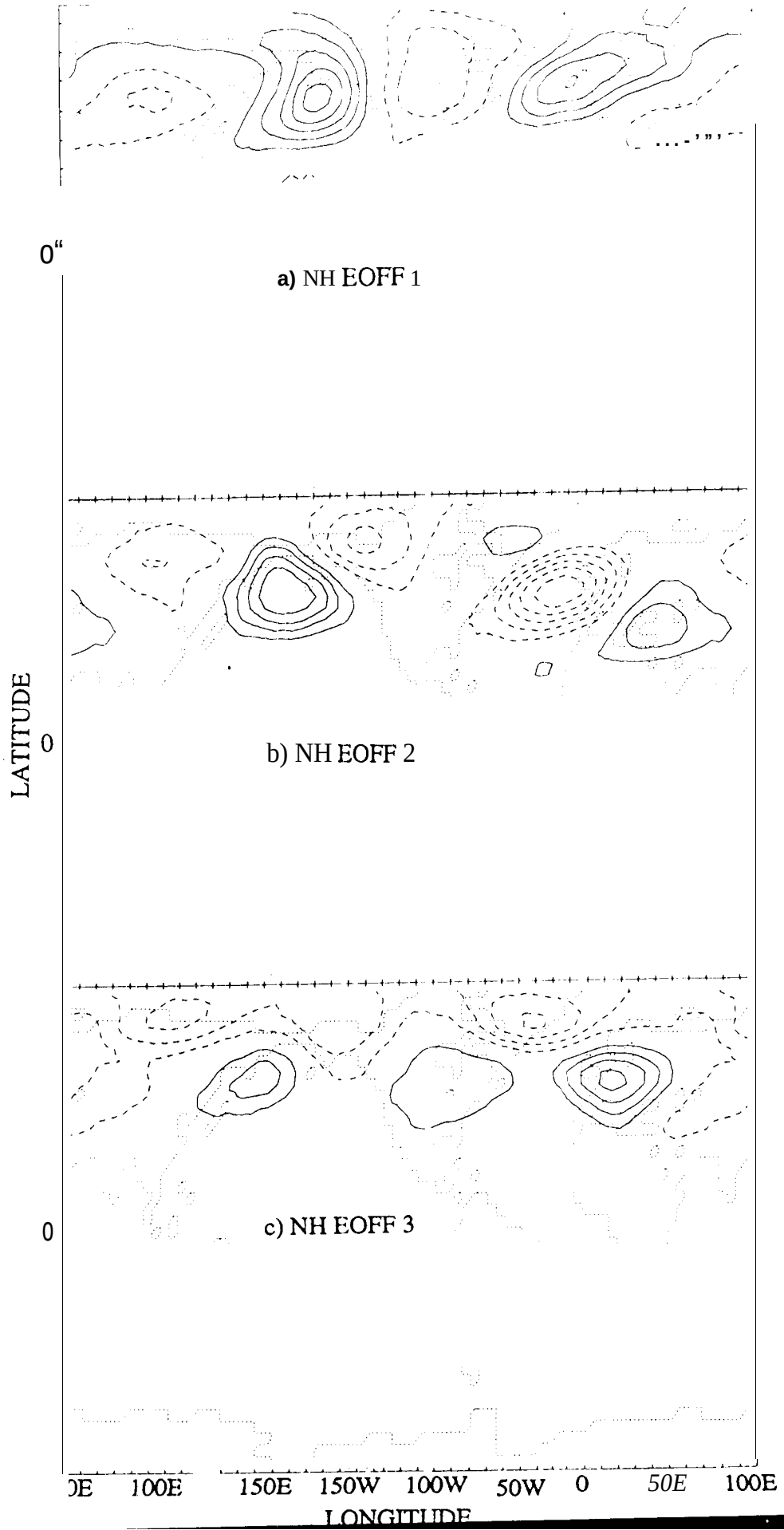
0"
a) NH EOFF 1
LATITUDE
0
b) NH EOFF 2
0
c) NH EOFF 3
0E
100E
150E
150W
100W
50W
0
50E
100E
LONGITUDE

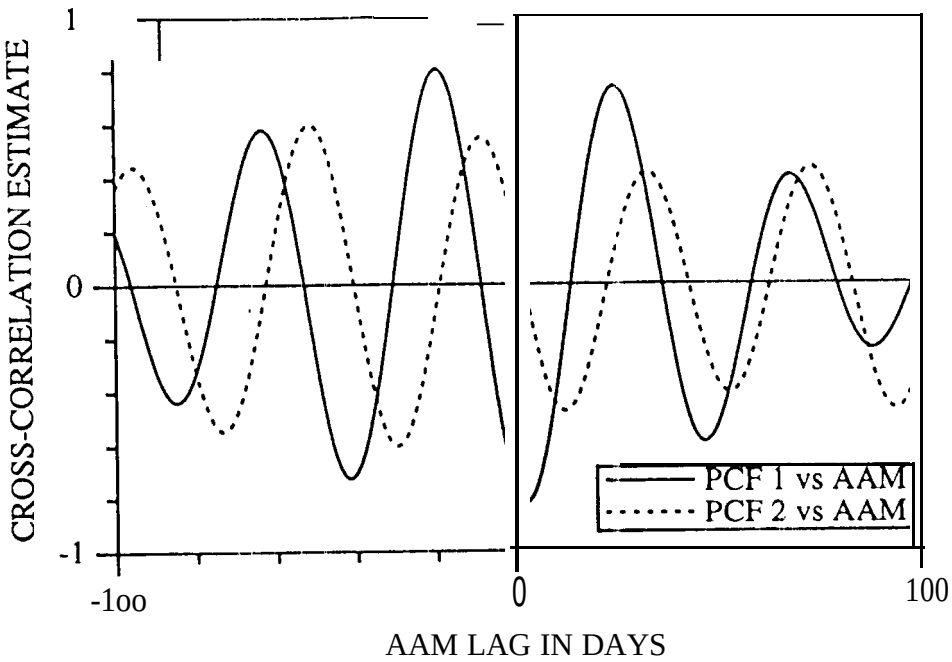
CROSS-CORRELATION ESTIMATE
1
0
-1
-1oo
0
100
PCF 1 vs AAM
PCF 2 vs AAM
AAM LAG IN DAYS

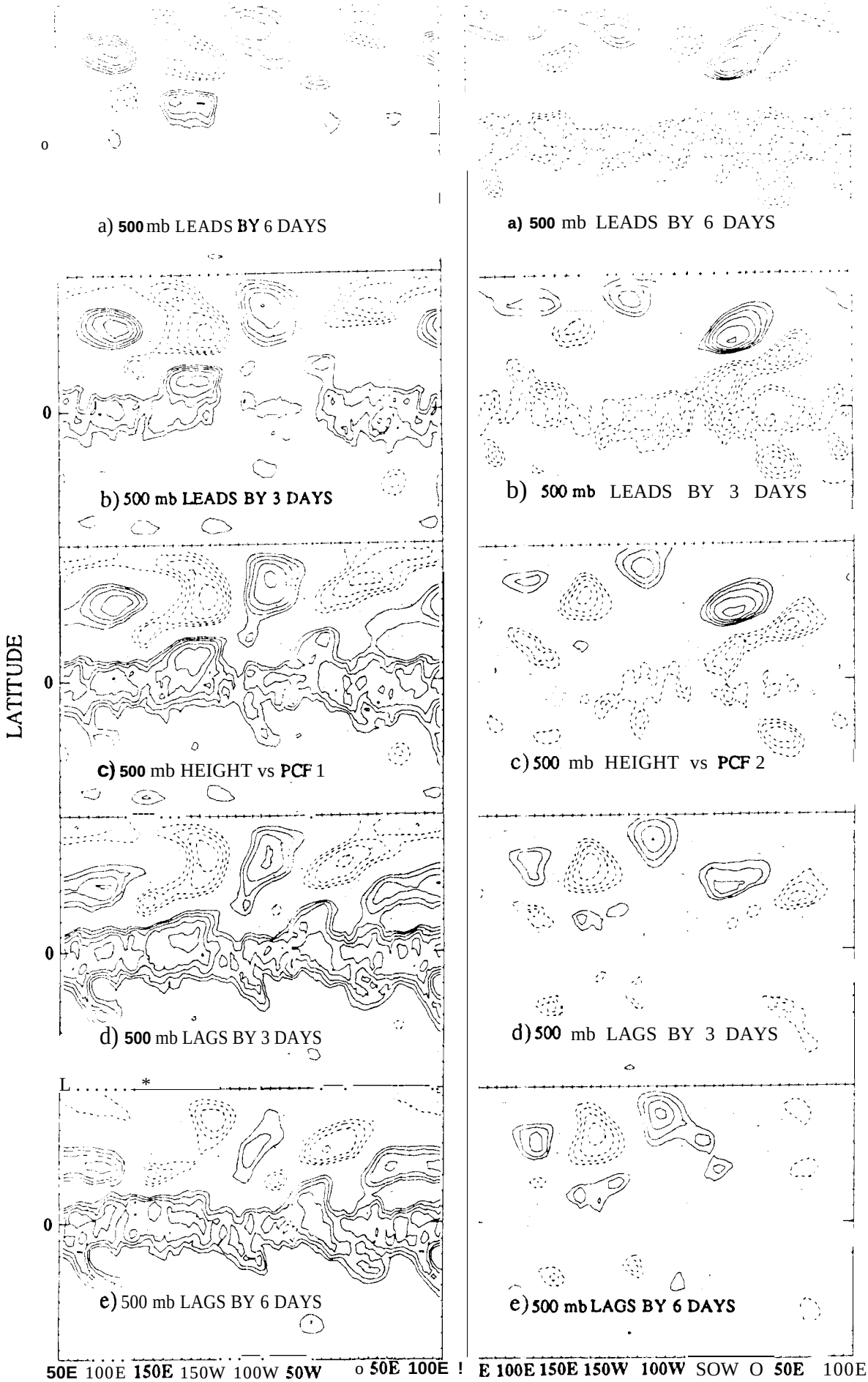
a) 500 mb LEADS BY 6 DAYS
a) 500 mb LEADS BY 6 DAYS
b) 500 mb LEADS BY 3 DAYS
b) 500 mb LEADS BY 3 DAYS
c) 500 mb HEIGHT vs PCF 1
c) 500 mb HEIGHT vs PCF 2
d) 500 mb LAGS BY 3 DAYS
d) 500 mb LAGS BY 3 DAYS
e) 500 mb LAGS BY 6 DAYS
e) 500 mb LAGS BY 6 DAYS
LATTITUDE
0
50E 100E 150E 150W 100W 50W
50E 100E 150E 150W 100W SOW O 50E 100E
LONGITUDE
LONGITUDE

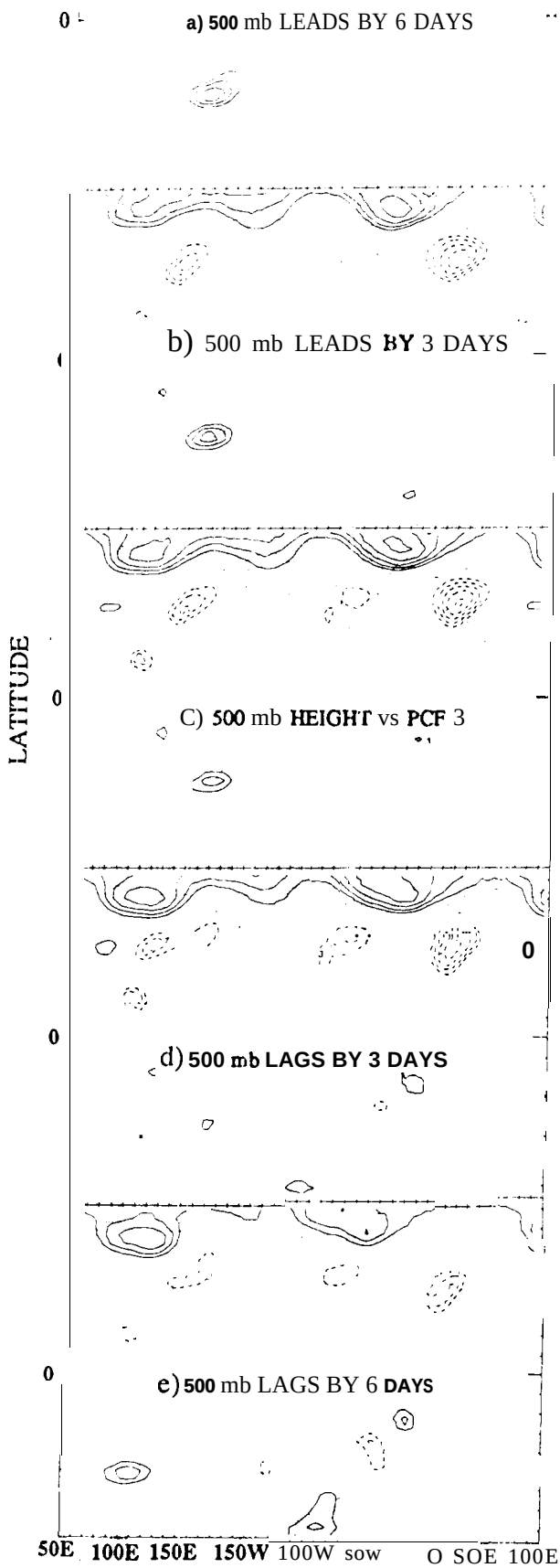
a) 500 mb LEADS BY 6 DAYS
b) 500 mb LEADS BY 3 DAYS
C) 500 mb HEIGHT vs PCF 3
d) 500 mb LAGS BY 3 DAYS
e) 500 mb LAGS BY 6 DAYS
LATITUDE
0
0
0
0
0
50E 100E 150E 150W 100W sow O SOE 100E
LONGITUDE

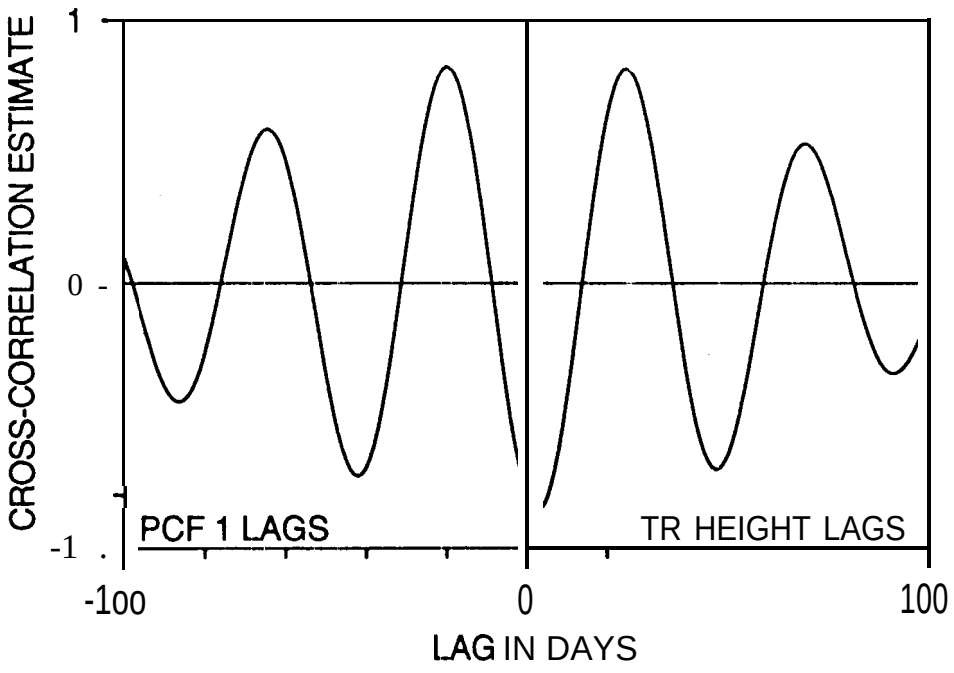
CROSS-CORRELATION ESTIMATE
1
0
-1
PCF 1 LAGS
TR HEIGHT LAGS
-100
0
100
LAG IN DAYS

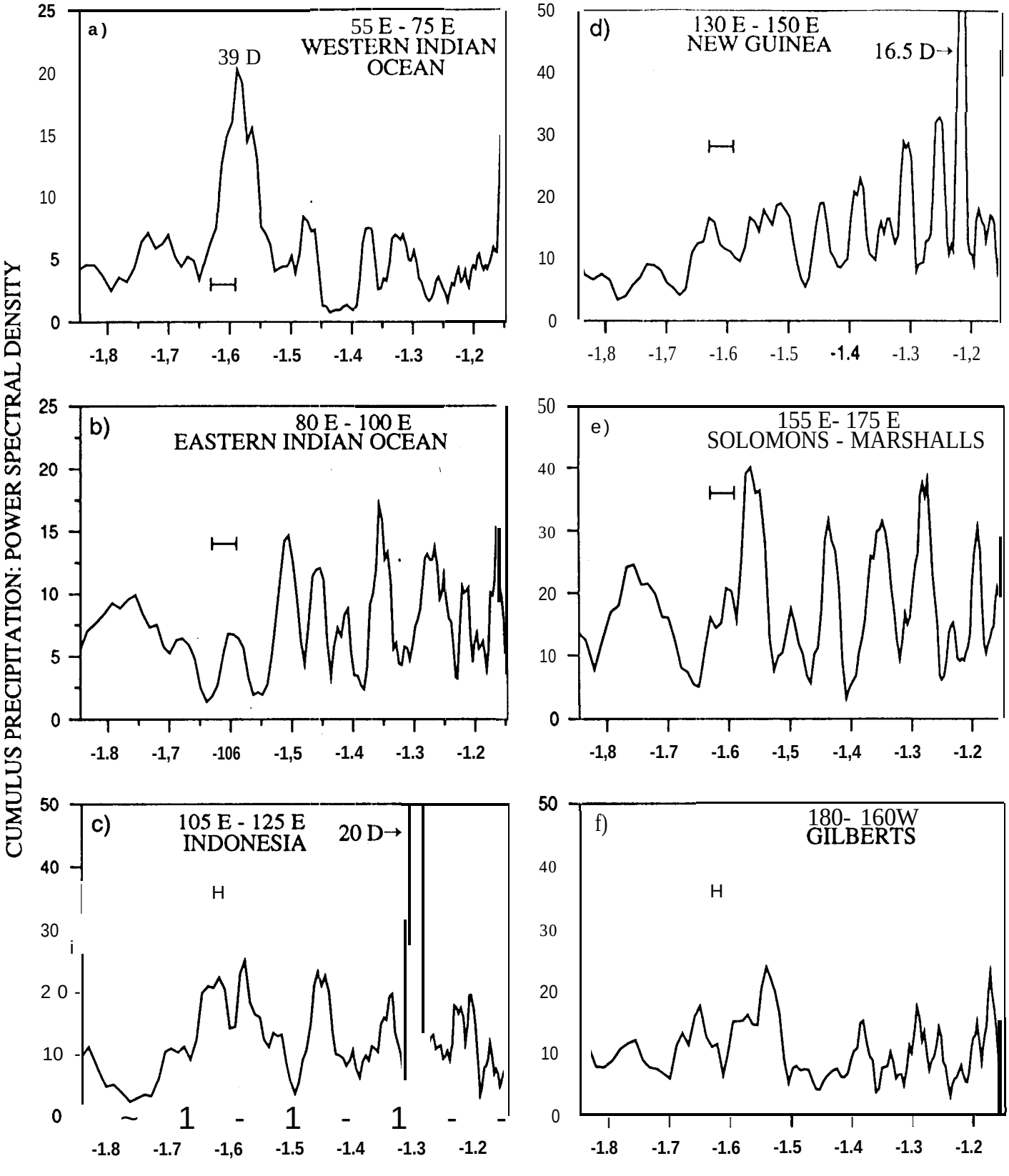
a)
55 E - 75 E
WESTERN INDIAN
OCEAN
39 D
b)
80 E - 100 E
EASTERN INDIAN OCEAN
c)
105 E - 125 E
INDONESIA
20 D→
d)
130 E - 150 E
NEW GUINEA
16.5 D→
e)
155 E- 175 E
SOLOMONS - MARSHALLS
f)
180- 160W
GILBERTS
CUMULUS PRECIPITATION: POWER SPECTRAL DENSITY
LOG10 (CYCLES/DAY)

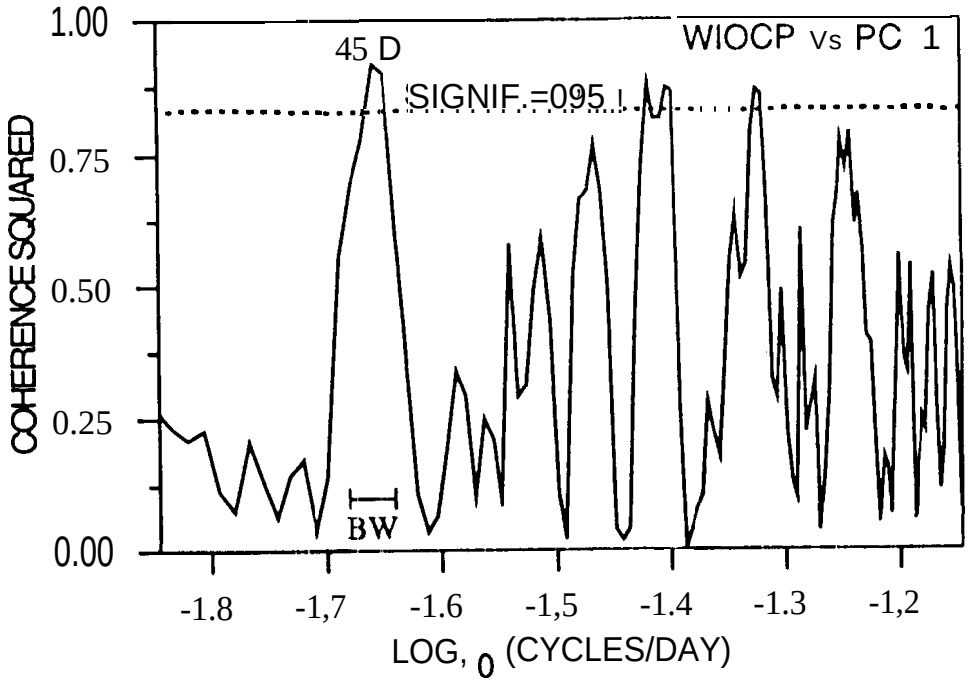
1.00
0.75
0.50
0.25
0.00
COHERENCE SQUARED
45 D
WIOCP Vs PC 1
SIGNIF.=095
BW
-1.8
-1,7
-1.6
-1,5
-1.4
-1.3
-1,2
LOG, 0 (CYCLES/DAY)

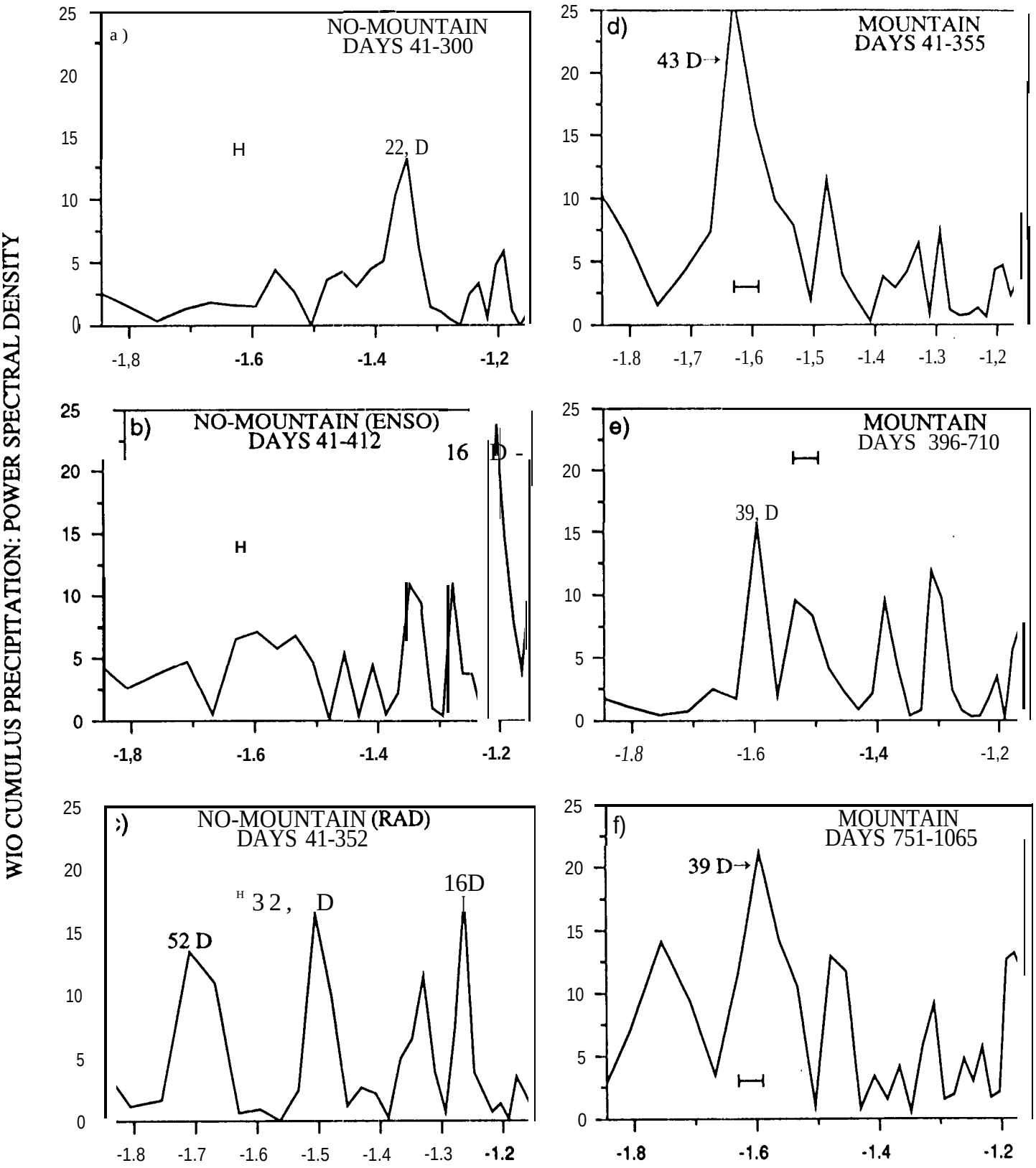
a)
NO-MOUNTAIN
DAYS 41-300
H
22, D
d)
MOUNTAIN
DAYS 41-355
43 D→
b)
NO-MOUNTAIN (ENSO)
DAYS 41-412
H
e)
MOUNTAIN
DAYS 396-710
39, D
NO-MOUNTAIN (RAD)
DAYS 41-352
H 32, D
52 D
16D
f)
MOUNTAIN
DAYS 751-1065
39 D→
WIO CUMULUS PRECIPITATION: POWER SPECTRAL DENSITY
LOG 10 (CYCLES/DAY)